

A hybrid dynamical extension of averaging and its application to the analysis of legged gait stability

The International Journal of
Robotics Research
2018, Vol. 37(2–3) 266–286
© The Author(s) 2018
Reprints and permissions:
sagepub.co.uk/journalsPermissions.nav
DOI: 10.1177/0278364918756498
journals.sagepub.com/home/ijr



Avik De¹, Samuel A Burden² and Daniel E Koditschek¹

Abstract

We extend a smooth dynamical systems averaging technique to a class of hybrid systems with a limit cycle that is particularly relevant to the synthesis of stable legged gaits. After introducing a definition of hybrid averageability sufficient to recover the classical result, we illustrate its applicability by analysis of first a one-legged and then a two-legged hopping model. These abstract systems prepare the ground for the analysis of a significantly more complicated two legged model: a new template for quadrupedal running to be analyzed and implemented on a physical robot in a companion paper. We conclude with some rather more speculative remarks concerning the prospects for further extension and generalization of these ideas.

Keywords

Legged robots, dynamics, motion control

1. Introduction

The emergence of physically motivated and mathematically tractable hybrid models (Burden et al., 2015, 2016; Johnson et al., 2016) offers the prospect of extending classical ideas and techniques of dynamical systems theory for application to new settings arising from the repeated making and breaking of contacts endemic to robotic mobility and manipulation. In this paper, we work at the intersection of a class of tractable hybrid legged locomotion models (Johnson et al., 2016) with a class of well-behaved hybrid limit cycle models (Burden et al., 2015) to generalize an initial result (De and Koditschek, 2015a) on the stability of “averageable” hybrid oscillators. Specifically, we extend a classical smooth dynamical averaging technique to a class of hybrid systems with a limit cycle that is particularly relevant to the synthesis of stable gaits.

We also present three applications of the new averaging result to prove stability of hybrid limit cycles, first for an isolated vertically hopping leg, then for two physically decoupled (but informationally coupled) vertically hopping legs exhibiting in-phase (“pronking”) and anti-phase (“bounding”) limiting phase offsets. In a companion paper, we use the same result to prove stability in a mechanically coupled pair of vertical hoppers (De and Koditschek, 2018), a model that provides remarkable insight into reflexive and feedback stabilization of these gaits on a physical quadruped machine. A list of important symbols used throughout the paper is given in Table 1.

1.1. Relation to prior literature

Classical averaging (Guckenheimer and Holmes, 1990, Ch. 4.1) yields a method of approximating (with error bounds) solutions of the T -periodic vector field (1) using the averaged vector field (3). As in the classical case, our new hybrid results guarantee equivalence in stability type to a simpler approximant (named the *averaged system*) of the system of interest. Specifically, we show that if the return map of the averaged system has a hyperbolic periodic orbit, then so does the original system, and additionally the linearizations of the return maps are ε^2 -close (and, thus, share the same eigenvalues and eigenvectors to $\mathcal{O}(\varepsilon)$).

This paper is also related to previous stability analyses of hybrid oscillators appearing in locomotion for a single vertical hopper (Koditschek and Buehler, 1991), as well as informationally coupled, physically decoupled vertical hoppers (Klavins and Koditschek, 2002; Klavins et al., 2000). Application of the hybrid averaging result in these instances yields a greater analytical simplification than has been possible before. In fact, we show in our analysis that the nonlinear stance dynamics in our vertical hopper (Section

¹Electrical and Systems Engineering, University of Pennsylvania, Philadelphia, PA, USA

²Electrical Engineering, University of Washington, Seattle, WA, USA

Corresponding author:

Avik De, Electrical and Systems Engineering, University of Pennsylvania, Pennovation Center, Building 6176, 3rd Floor, 3401 Grays Ferry Avenue, Philadelphia, PA 19146, USA.

Email: avik@seas.upenn.edu

4.1) can be reduced to an “averaged” continuous dynamics that appears as a phase-independent proportional controller on the energy (43). Whereas single-vertical-hopper stability results have been obtained before without averaging (e.g. Koditschek and Buehler, 1991), the more complex latter instance (informationally coupled vertical hoppers) has heretofore only been analyzed in the context of a simplified, integrable Hamiltonian (i.e. lossless) stance model (Klavins and Koditschek, 2002, equation (20)). Integrable stance dynamics allowed for a discrete return map control strategy (Klavins and Koditschek, 2002, equation (26)), but cannot be extended to more general (e.g. two degrees of freedom (DOFs) or greater) non-integrable dynamical templates such as the so-called spring-loaded inverted pendulum (SLIP) (Saranli et al., 1998). Hybrid averaging allows us to analyze with relative ease the general (non-Hamiltonian) paired vertical hopper plant model obviating the need to integrate the time-varying flow and, rather, requiring only examination of its reduced-dimensional, simplified, averaged approximant (Section 4). Formal stability analyses of such non-integrable 2-DOF models has not been achieved thus far in the literature, leading past researchers to resort to numerical methods (Poulakakis, 2006; Shahbazi and Lopes, 2016). Further work is currently underway to use hybrid averaging in conjunction with observations on time-reversal symmetry (Altendorfer et al., 2004; Razavi et al., 2016) to provide stability analyses of still higher DOF coupled systems including the SLIP template (Full and Koditschek, 1999) and its anchoring physical models that encode fore–aft motion as well as vertical travel.

1.2. Contributions and organization

After proving the formal result, we first apply it to a simple 1-DOF vertical hopper to provide a lightweight illustration of how its hypotheses, inherited (and rendered somewhat more intricate by extension) from the classical setting, extend beyond the narrow sufficient conditions first articulated in De and Koditschek (2015a) and review how the limit cycle it guarantees represents the gait of a single-legged runner. We then apply the result to a pair of such vertical hoppers coupled via a three-parameter family of feedback gains. Two different parameter settings require two rather different strategies for its application and yield two different limit cycles, one exhibiting an in-phase and the other an anti-phase relation between the two hoppers.

In the companion paper (De and Koditschek, 2018), we further couple these vertical hoppers mechanically to reveal a simplified model of quadrupedal running that we call the “slot-hopper” template (using the terminology of Full and Koditschek (1999)). In that more intricate setting, we show how further effort in the application of this paper’s results yields a complete analysis of virtual bipedal gaits for quadrupedal running-in-place wherein the in-phase limit cycle encodes stable pronking-in-place while the anti-phase

limit cycle encodes stable bounding-in-place anchored by a physical robot.

Section 2 first introduces and proves the averaging result for hybrid systems in a single domain with non-overlapping guards and fixed time-of-flow (Theorem 2). Subsequently, in Theorem 3, we provide a condition under which the more general case (where the flow time between resetting is not constant) reduces to the former case (by appropriately redefining the reset map).

Section 3 introduces a motivational physical model on which to demonstrate and offer something of a tutorial on how to use our results. We choose a pair of vertically constrained hoppers for their dynamical simplicity (in this paper we leave them physically uncoupled) notwithstanding their applicability to the understanding of virtual bipedal gaits exhibited by physical bipedal or quadrupedal machines.

Section 4 illustrates the utility of this result from Section 2 to the stability analysis of the models introduced in Section 3 by application of Theorem 2 or 3. We offer accompanying simulation results in Section 5 suggesting the physical relevance of this theory that will be demonstrated in the companion paper (De and Koditschek, 2018).

Section 6 concludes with a discussion of the limitations in the presently required conditions and some more speculative remarks on their relaxation as well as extensions to facilitate applications to higher-dimensional problems.

2. Hybrid averaging

2.1. Classical averaging (background)

Following (Guckenheimer and Holmes, 1990), consider a time-varying system

$$\dot{x} = \varepsilon f(x, t, \varepsilon); \quad x \in \mathcal{U} \subset \mathbb{R}^n, \quad 0 < \varepsilon \ll 1 \quad (1)$$

The averaged system is defined as

$$\dot{y} = \varepsilon \frac{1}{T} \int_0^T f(y, t, 0) dt =: \varepsilon \bar{f}(y) \quad (2)$$

Note that y is used instead of x to make clear that these vector fields act on different coordinates. We describe the necessary coordinate change below.

Theorem 1 (Smooth averaging theorem (Guckenheimer and Holmes, 1990)). *There exists a C^r change of coordinates $x = y + \varepsilon w(y, t, \varepsilon)$ under which (1) becomes*

$$\dot{y} = \varepsilon \bar{f}(y) + \varepsilon^2 f_1(y, t, \varepsilon) \quad (3)$$

Moreover,

- (i) *If $x(t)$ and $y(t)$ are solutions of (1) and (2) with initial conditions $x(0)$, $y(0)$ respectively, and $|x(0) - y(0)| = \mathcal{O}(\varepsilon)$, then $|x(t) - y(t)| = \mathcal{O}(\varepsilon)$ on a time scale $t \sim 1/\varepsilon$.*
- (ii) *If f is periodic with period T , and if p_0 is a hyperbolic equilibrium of (2), then there exists $\varepsilon_0 > 0$ such that,*

Table 1. Important symbols used throughout the paper, in order of appearance.

Symbol	Brief description	Ref.	Symbol	Brief description	Ref.
$\varepsilon \in \mathbb{R}_+$	Averaging parameter	Section 2	$F : \mathcal{X} \rightarrow T\mathcal{X}$	Stance vector field	Section 2
$f : \mathcal{X} \rightarrow T\mathcal{X}_2$	Slow vector field	Section 2	$\bar{f} : \mathcal{X}_2 \rightarrow T\mathcal{X}_2$	Averaged vector field	Section 2
$\bar{R} : \mathcal{X}_2 \rightarrow \mathcal{X}_2$	Slow coordinate reset	Section 2	$\gamma : \mathcal{X} \rightarrow \mathbb{R}$	Event function	Section 2
$\mathcal{G} \subset \mathcal{X}$	Guard set	Section 2	$\bar{P} : \mathcal{X}_2 \rightarrow \mathcal{X}_2$	Averaged return map	Section 2
$g \in \mathbb{R}_+$	Acceleration due to gravity	(29)	$z_i \in \mathbb{R}$	Physical hip height	Section 3.2
$\bar{s} \in \mathbb{R}^4$	State vector (Figure 3 model)	Section 3.2	$u_i : \mathcal{X} \rightarrow \mathbb{R}$	Hip control input	(31)
$\omega \in \mathbb{R}_+$	Stance spring frequency	(32)	$p \in \mathbb{R}^2 \rightarrow \mathbb{R}^2$	Stance phase vector	(32)
$\rho \in \mathbb{R}_+$	Nominal leg length	(32)	$a_i \in \mathbb{R}_+$	Hip energy (liftoff velocity)	(33)
$\psi_i \in \Psi \subset \mathbb{R}_+$	Hip phase	(34)	$\omega_f : \mathbb{R}_+ \rightarrow \mathbb{R}_+$	Flight frequency	(35)
$\delta \in \mathbb{R}$	Phase difference	(36)	$\beta \in \mathbb{R}_+$	Stance damping	(37)
$v_i : \mathcal{X} \rightarrow \mathbb{R}$	Nonlinear part of control	(37)	$w_i : \mathcal{X} \rightarrow \mathbb{R}$	Frequency control input	(37)
$k_a \in \mathbb{R}_+$	Vertical gain	(37)	$k_p, k_d \in \mathbb{R}_+$	Coordination control gains	(38), (39)
$K : \mathbb{R}^4 \rightarrow \mathbb{R}^4$	Bipedal symmetry	(48)	$\bar{K} : \mathbb{R}^{3 \times 3}$	Slow-coordination symmetry	(49)
(ψ_1, a_1)	“Single” average vector	Section 4.1	$(\psi_1, a_1, a_2, \delta)$	“Decoupled” average vector	Sections 4.2–4.3

for all $0 < \varepsilon \leq \varepsilon_0$, Equation (1) possesses a unique hyperbolic periodic orbit $\gamma_\varepsilon(t) = p_0 + \mathcal{O}(\varepsilon)$, of the same stability type as p_0 .

Remark 1. The statement (i) does not depend on the periodicity assumption made in Guckenheimer and Holmes (1990), but (ii) does. Further, we emphasize that we do not compare the behaviors of (1) and (2) directly; instead, we change coordinates for the original vector field from x to y , and then compare the behavior of the original system in the new coordinates (3) to the “model averaged system” (2).

In the following, we replicate the proof of Theorem 1 from Guckenheimer and Holmes (1990), so that unfamiliar readers have an accessible reference for this result, which our novel contributions depend heavily on.

Proof (from Guckenheimer and Holmes (1990)). First, we compute the change of coordinates explicitly. Let

$$f(x, t, \varepsilon) = \bar{f}(x) + \tilde{f}(x, t, \varepsilon) \quad (4)$$

be split into its mean, \bar{f} , and oscillating, \tilde{f} , parts. Let

$$x = h(y) := y + \varepsilon w(y, t, \varepsilon) \quad (5)$$

without yet choosing w . Differentiating the equation above and using (1) and (4), we have

$$\begin{aligned} (I + \varepsilon D_y w) \dot{y} &= \dot{x} - \varepsilon \frac{\partial w}{\partial t} \\ &= \varepsilon \bar{f}(y + \varepsilon w) + \varepsilon \tilde{f}(y + \varepsilon w, t, \varepsilon) - \varepsilon \frac{\partial w}{\partial t} \end{aligned}$$

or (expanding in powers of ε , and choosing w such that $\frac{\partial w}{\partial t} := \tilde{f}(y, t, 0)$),¹

$$\begin{aligned} \dot{y} &= \varepsilon (I + \varepsilon D_y w)^{-1} \left[\bar{f}(y) + \varepsilon D_y \bar{f} \cdot w(y, t, 0) \right. \\ &\quad \left. + \tilde{f}(y, t, 0) + \varepsilon \frac{\partial \tilde{f}}{\partial \varepsilon}(y, t, 0) - \tilde{f}(y, t, 0) + \mathcal{O}(\varepsilon^2) \right] \\ &= \varepsilon (I - \varepsilon D_y w) \left[\bar{f}(y) + \varepsilon D_y \bar{f} \cdot w(y, t, 0) \right. \\ &\quad \left. + \varepsilon \frac{\partial \tilde{f}}{\partial \varepsilon}(y, t, 0) \right] + \mathcal{O}(\varepsilon^3) \\ &= \varepsilon \bar{f}(y) + \varepsilon^2 \left[\varepsilon D_y \bar{f} \cdot w(y, t, 0) - D_y w(y, t, 0) \bar{f}(y) \right. \\ &\quad \left. + \frac{\partial \tilde{f}}{\partial \varepsilon}(y, t, 0) \right] + \mathcal{O}(\varepsilon^3) \\ &=: \varepsilon \bar{f}(y) + \varepsilon^2 f_1(y, t, \varepsilon) \end{aligned} \quad (6)$$

as required by (3).

We use a version of Gronwall’s lemma (see Guckenheimer and Holmes, 1990 for details) to compare the solutions of (2) and (3). If $y(t)$ and $y_\varepsilon(t)$ are their respective solutions, the lemma states that if $|y(0) - y_\varepsilon(0)| = \mathcal{O}(\varepsilon)$, then $|y_\varepsilon(t) - y(t)| = \mathcal{O}(\varepsilon)$ for $t \in [0, \frac{1}{\varepsilon L}]$. Using the coordinate change (5), we know that

$$|x(t) - y_\varepsilon(t)| = \varepsilon w(y_\varepsilon(t), t, \varepsilon) = \mathcal{O}(\varepsilon)$$

and using the triangle inequality,

$$|x(t) - y(t)| \leq |x(t) - y_\varepsilon(t)| + |y_\varepsilon(t) - y(t)| = \mathcal{O}(\varepsilon)$$

and we obtain the desired result (i).

To prove (ii), we again follow the proof strategy of Guckenheimer and Holmes (1990), but provide significantly more detail as well as correct some typos in the original. We also enumerate the steps in order to better reference them in the following text.

- (a) We consider the Poincaré maps P_0 and P_ε associated with (2) and (3). Rewriting these latter systems as

$$\dot{y} = \varepsilon \bar{f}(y), \quad \dot{\theta} = 1 \quad (7)$$

$$\dot{y} = \varepsilon \bar{f}(y) + \varepsilon^2 f_1(y, \theta, \varepsilon), \quad \dot{\theta} = 1 \quad (8)$$

where $(y, \theta) \in \mathbb{R}^n \times \mathbb{S}^1$, and $\mathbb{S}^1 = \mathbb{R}/T$ is a circle of length T . We define a global cross-section $\Sigma := \{(y, \theta) : \theta = 0\}$, and the first return or time T Poincaré maps $P_0 : \mathcal{U} \rightarrow \Sigma, P_\varepsilon : \mathcal{U} \rightarrow \Sigma$ are then defined for (7) and (8) as the flow maps associated with a time- T flow of each of the time-varying dynamics with initial condition $t = 0$, where $\mathcal{U} \subseteq \Sigma$ is some open set.

- (b) If p_0 is a hyperbolic equilibrium of (2), then $\bar{f}(p_0) = 0$. Using (Hirsch et al., 1974, 300), the spatial Jacobian of the flow around and equilibrium is that of a linear time-invariant system, and so^{2,3}

$$DP_0(p_0) = e^{\varepsilon T D\bar{f}(p_0)} = I + \varepsilon T D\bar{f}(p_0) + \mathcal{O}(\varepsilon^2) \quad (9)$$

- (c) Note that P_ε is ε -close⁴ to P_0 since T is fixed independent of ε , using the result of (i).⁵ Next we show that $DP_\varepsilon(p_0) = DP_0(p_0) + \mathcal{O}(\varepsilon^2)$. For this, consider the time-invariant vector field corresponding to (8),

$$\begin{bmatrix} \dot{y} \\ \dot{\theta} \end{bmatrix} = \begin{bmatrix} \varepsilon \bar{f}(y) + \varepsilon^2 f_1(y, \theta, \varepsilon) \\ 1 \end{bmatrix},$$

and define its time- t flow from initial condition (y, θ) as $\Phi_\varepsilon(y, \theta, t)$, versus the corresponding flow $\Phi_0(y, \theta, t)$ for (7). Note that, by definition, $P_\varepsilon(p) := \pi_y \Phi_\varepsilon(p, 0, T)$, where π_y is the projection to the y -coordinates. Following (Hirsch et al., 1974, 300) to compute the spatial derivative of the flow, we obtain the linear time-varying system where $A(t) := D\Phi_\varepsilon(y(t), 0, t)$,

$$\dot{A}(t) = \begin{bmatrix} \varepsilon D\bar{f} + \varepsilon^2 D_y f_1 & \varepsilon^2 D_\theta f_1 \\ 0 & 0 \end{bmatrix} A(t).$$

We can solve this linear time-varying system using the Peano–Baker series. As we are only interested in the top left block, we can compute it at p_0 ,

$$\begin{aligned} DP_\varepsilon(p_0) &= I + \varepsilon \int_0^T D\bar{f}(\Phi_\varepsilon(p_0, \theta, t)) dt + \mathcal{O}(\varepsilon^2) \\ &= I + \varepsilon \int_0^T \left[D\bar{f}(\Phi_\varepsilon(p_0, \theta, t)) - D\bar{f}(\Phi_0(p_0, \theta, t)) \right. \\ &\quad \left. + D\bar{f}(\Phi_0(p_0, \theta, t)) \right] dt + \mathcal{O}(\varepsilon^2) \\ &\stackrel{\star}{=} I + \varepsilon T D\bar{f}(p_0) + \varepsilon \int_0^T \left[D\bar{f}(\Phi_\varepsilon(p_0, \theta, t)) \right. \\ &\quad \left. - D\bar{f}(\Phi_0(p_0, \theta, t)) \right] dt + \mathcal{O}(\varepsilon^2) \\ &\stackrel{\textcircled{0}}{=} DP_0(p_0) + \varepsilon \int_0^T \left[D\bar{f}(\Phi_\varepsilon(p_0, \theta, t)) \right. \\ &\quad \left. - D\bar{f}(\Phi_0(p_0, \theta, t)) \right] dt + \mathcal{O}(\varepsilon^2) \end{aligned}$$

where we used the fact that $\Phi_0(p_0, \theta, t) \equiv p_0$ for step \star . From (i), for $\theta \in [0, T]$ we know that $\|\Phi_\varepsilon(p_0, \theta, t) - \Phi_0(p_0, \theta, t)\| = \mathcal{O}(\varepsilon) \implies \Phi_\varepsilon(p_0, \theta, t) = \Phi_0(p_0, \theta, t) + \mathcal{O}(\varepsilon)$. In addition, $D\bar{f}$ is Lipschitz continuous and so $D\bar{f}(\Phi_\varepsilon(p_0, \theta, t)) = D\bar{f}(\Phi_0(p_0, \theta, t)) + \mathcal{O}(\varepsilon)$. Using this in the block equation above, we have $DP_\varepsilon(p_0) = DP_0(p_0) + \mathcal{O}(\varepsilon^2)$.

- (d) Consider the function $\zeta(p, \varepsilon) := \frac{1}{\varepsilon}(P_\varepsilon(p) - p)$,⁶ such that $D_p \zeta = \frac{1}{\varepsilon}(e^{\varepsilon T Df(p)} - I)$, and $\lim_{\varepsilon \rightarrow 0} D_p \zeta = T D\bar{f}(p)$. Note that zeros of ζ correspond to fixed points of P_ε , and that $D_p \zeta(p_0, \varepsilon) = T D\bar{f}(p_0)$ is invertible. The implicit function theorem (IFT) implies that the zeros of $D_p \zeta$ form a smooth curve $(p_\varepsilon, \varepsilon) \in \mathbb{R}^n \times \mathbb{R}$. Thus, p_ε are fixed points of P_ε and, further, $p_\varepsilon = p_0 + \mathcal{O}(\varepsilon)$.
- (e) Putting together the prior steps, we see that

$$\begin{aligned} DP_\varepsilon(p_\varepsilon) &= \exp[\varepsilon T (Df(p_\varepsilon) + \varepsilon^2 Df_1(p_\varepsilon))] \\ &= \exp[\varepsilon T Df(p_0) + \mathcal{O}(\varepsilon^2) + \varepsilon^2 T Df_1(p_\varepsilon)] \\ &= \exp[\varepsilon T Df(p_0)] + \mathcal{O}(\varepsilon^2) \end{aligned}$$

or $DP_\varepsilon(p_\varepsilon) = DP_0(p_0) + \mathcal{O}(\varepsilon^2)$.

- (f) Owing to (d) and (e), the eigenvalues of $DP_\varepsilon(p_\varepsilon)$ are ε^2 close to those of $DP_0(p_0)$. Consequently, the stability properties of P_ε at its fixed point, p_ε , are the same as that of P_0 at its fixed point, p_0 .

Thus, (8) has a periodic orbit ε -close to p , and via the change of coordinates (5), Equation (1) has a similar orbit. \square

2.2. Switching systems (fixed-interval reset)

The smoothness assumption of Theorem 1 precludes its application to legged locomotion, since the making and breaking of contacts with the environment is a crucial component of this domain. We begin by introducing (in this subsection) discrete “reset” maps that interrupt the continuous flow of (1) at fixed time intervals, which fall under the umbrella of “switching” systems (Van Der Schaft and Schumacher, 2000), and in Section 2.3 we generalize to a state-dependent event-based reset, which typically arises in legged locomotion (Johnson et al., 2016).

2.2.1. Averaging coordinate change. Even though not required for the proof of Theorem 1, we will find it useful to delve deeper into the structure of the coordinate change (5). As pointed out in the proof of Theorem 1, w is a solution to the partial differential equation (PDE) $\frac{\partial w}{\partial t} := \tilde{f}(y, t, 0)$. From this we make the following observations:

- w does not depend on ε ;
- the base value of w at $t = 0$ is not yet constrained, so we are free to choose (as in Guckenheimer and Holmes, 1990, Example 1, Section 4.2)

$$w(y, 0, \varepsilon) \equiv 0 \text{ for all } y, \varepsilon; \quad (10)$$

- h in (5) is a good change of coordinates for sufficiently small $\varepsilon > 0$, since it is ε -close to the identity map;

- since the right-hand side of $\frac{\partial w}{\partial t} := \tilde{f}(y, t, 0)$ does not depend on w , and also since y is held fixed while taking the partial derivative with respect to t , this PDE can be solved by simply integrating over t , i.e.

$$w(y, t, \varepsilon) := \int_0^t \tilde{f}(y, \sigma, 0) d\sigma \quad (11)$$

is a solution of (5).

We illustrate in several examples in (De, 2017) that (11) is indeed a coordinate change from (1) to (3).

Lemma 1 (Endpoint behavior of averaging coordinate change). *At $t = T$, the coordinate change w has the properties*

- (i) $w(y, T, \varepsilon) = 0$; and
- (ii) $D_y w(y, T, \varepsilon) = 0$.

Proof. We have

$$\begin{aligned} w(y, T, \varepsilon) &\stackrel{(5)}{=} \int_0^T \tilde{f}(y, \sigma, 0) d\sigma \\ &\stackrel{(4)}{=} \int_0^T f(y, \sigma, 0) d\sigma - T\bar{f}(y) \stackrel{(2)}{=} 0 \end{aligned}$$

by the definition of \bar{f} . Similarly,

$$\begin{aligned} D_y w(y, T, \varepsilon) &\stackrel{(5)}{=} \int_0^T D_y \tilde{f}(y, \sigma, 0) d\sigma \\ &\stackrel{(4)}{=} \int_0^T D_y f(y, \sigma, 0) d\sigma - T D_y \bar{f}(y) \\ &= D_y \left(\int_0^T f(y, \sigma, 0) d\sigma - T\bar{f}(y) \right) \stackrel{(2)}{=} 0, \end{aligned}$$

where, in the penultimate step, we switched the order of the derivative and the integral. \square

We remark here that the result of Lemma 1 is unsurprising: the intuitive purpose of \tilde{f} is to capture the “deviation” between the original vector field f (1) and \bar{f} (2), and we should expect (from the definition of the “average” vector field) that the deviation integrates to 0.

2.2.2. Switching systems (constant flow time). Now suppose that instead of a smooth periodic system, we have a switching system with the flow of (1) punctuated by a reset, R (acting on the original x -coordinates). We assume for this section that the reset acts after a fixed flow time T of (1), and relax this assumption in the next section.

Theorem 2 (Switching averaging theorem). *Given the “original” and “averaged” switching systems of the forms*

$$\dot{x} = \varepsilon f(x, t, \varepsilon), \quad \dot{\theta} = 1, \quad x(T^+) = R(x(T)) \quad (12)$$

$$\dot{y} = \varepsilon \bar{f}(y), \quad \dot{\theta} = 1, \quad y(T^+) = R(y(T)) \quad (13)$$

where R is allowed to vary with ε , T^+ refers to a limit from the right, and θ is reset to 0 by the switching event:

- (i) the C^r (for $r \geq 2$) reset R satisfies: (a) $D_x R(x) = S_0 + \varepsilon S_1(x, \varepsilon)$ (with constant S_0), (b) S_0 is invertible, and its unity eigenvalues have diagonal Jordan blocks (i.e. unity eigenvalues have algebraic multiplicity 1); and
- (ii) there is a point p_0 such that: (a) it is an equilibrium of \bar{f} , (b) $R(p_0) = p_0$, and (c) the averaged return map is hyperbolic at p_0 ;

there exists $\varepsilon_0 > 0$ such that, for all $0 < \varepsilon \leq \varepsilon_0$, Equation (12) possesses a unique hyperbolic periodic orbit, of the same stability type as p_0 .

Proof. First, we apply the C^r coordinate change (5). As shown in the proof of Theorem 1(i), w converts the continuous dynamics in (12) to take the form of (3). Define the reset after the averaging coordinate change (5),

$$R_y := h^{-1} \circ R \circ h, \quad (14)$$

and convert (12) into the switching system

$$\begin{aligned} \dot{y} &= \varepsilon \bar{f}(y) + \varepsilon^2 f_1(y, \theta, \varepsilon), \quad \dot{\theta} = 1, \\ y(T_+) &= R_y(y(T)), \end{aligned} \quad (15)$$

where $(y, \theta) \in \mathbb{R}^n \times \mathbb{S}^1$, and $\mathbb{S}^1 = \mathbb{R}/T$ is a circle of length T . We know that the continuous flow of (15) can be approximated by (2) after changing coordinates; but we need to check how R_y and R are related using (14).

First, note that since R_y only acts on $y(T)$, and since the time dynamics in (15) are decoupled, we only ever need to compute $R_y(y(T))$, and $D_y R_y(y(T))$. From (5) and (14),

$$\begin{aligned} R_y(y(T)) &= R(x(T)) - \varepsilon w(x(0), 0, \varepsilon) \\ &\stackrel{(10)}{=} R(x(T)) = R(y(T)), \end{aligned} \quad (16)$$

where we used Lemma 1 to observe that $x(T) = y(T) + \varepsilon w(y(T), T, \varepsilon) = y(T)$ for the last equality, and where $T_+ = 0$ after the reset. Similarly, for the spatial Jacobian, first note that $D_y w(y, 0, \varepsilon) = 0$ from the assertion (10) for each $y(0)$. Then,

$$\begin{aligned} D R_y(y(T)) &= D R(x(T)) [I + \varepsilon D_y w(y(T), T, \varepsilon)] \\ &= D R(y(T)), \end{aligned}$$

where we used Lemma 1 for the last step.

The remainder of this proof follows closely the proof of Theorem 1 (ii), and we refer to those steps when convenient. Consider the Poincaré maps P_0, P_ε , and associated with (13) and (15). Define a section $\Sigma := \{(y, \theta) : \theta = 0\}$, and the first return or time T Poincaré maps $P_0 : \mathcal{U} \rightarrow \Sigma$, $P_\varepsilon : \mathcal{U} \rightarrow \Sigma$ are then defined for (13) and (15) as the flow maps associated with a time- T flow of each of the time-varying dynamics, with initial condition $t = 0$, composed with their respective resets

$$P_0 := R \circ Q_0, \quad P_\varepsilon := R_y \circ Q_\varepsilon,$$

where $\mathcal{U} \subseteq \Sigma$ is some open set, and Q_0, Q_ε are the time- T flows.

As shown in steps (b)–(c) in the proof of Theorem 1(ii), $DQ_0(p_0) = \exp[\varepsilon TD\bar{f}(p_0)]$, and $DQ_\varepsilon(p_0) = DQ_0(p_0) + \mathcal{O}(\varepsilon^2)$. In addition, as shown in step (c), the fundamental averaging result Theorem 1(i) shows that $Q_\varepsilon(p_0) = p_0 + \mathcal{O}(\varepsilon)$. Now incorporating the reset,

$$\begin{aligned}
DP_\varepsilon(p_0) &= DR(Q_\varepsilon(p_0)) \cdot DQ_\varepsilon(p_0) \\
&= DR(p_0 + \mathcal{O}(\varepsilon)) \cdot DQ_\varepsilon(p_0) \\
&= (S_0 + \varepsilon S_1(p_0 + \mathcal{O}(\varepsilon))) DQ_\varepsilon(p_0) \\
&\stackrel{\star}{=} (S_0 + \varepsilon S_1(p_0) + \mathcal{O}(\varepsilon^2)) DQ_\varepsilon(p_0) \\
&= (S_0 + \varepsilon S_1(p_0)) DQ_0(p_0) + \mathcal{O}(\varepsilon^2) \\
&= DR(p_0) DQ_0(p_0) + \mathcal{O}(\varepsilon^2) \\
&= DP_0(p_0) + \mathcal{O}(\varepsilon^2)
\end{aligned} \tag{17}$$

where for the step \star , we used the fact that S_1 is Lipschitz continuous.

By the hypotheses in the statement of Theorem 2(ii), we know that P_0 has a fixed point at p_0 , but we need to show that P_ε has a fixed point that is close. From the block equation above, $DP_\varepsilon(p_0) = S_0 + \varepsilon(S_1 + TD\bar{f}(p_0)) + \mathcal{O}(\varepsilon^2)$. By passing to the Jordan form, without loss of generality we assert that $S_0 = V \begin{bmatrix} I_m & 0 \\ 0 & U \end{bmatrix} V^{-1}$ (using the hypothesis that “1” eigenvalues have algebraic multiplicity 1 from Theorem 2(i)), where U does not have a unity eigenvalue. Now let $E(\varepsilon) := V \begin{bmatrix} I_{m/\varepsilon} & 0 \\ 0 & I_{n-m} \end{bmatrix} V^{-1}$. Define $\zeta(p, \varepsilon) = E(\varepsilon)(P_\varepsilon(p) - p)$. Note that $\zeta(p, 0) = 0$, and letting $\tilde{S}_1 := S_1 + TD\bar{f}(p_0)$

$$\begin{aligned}
&V^{-1}D_p\zeta(p_0, \varepsilon)V \\
&= V^{-1}E(DP_\varepsilon - I)V = \begin{bmatrix} I_{m/\varepsilon} & 0 \\ 0 & I_{n-m} \end{bmatrix} (V^{-1}DP_\varepsilon V - I) \\
&= \begin{bmatrix} I_{m/\varepsilon} & 0 \\ 0 & I_{n-m} \end{bmatrix} \left(\begin{bmatrix} I_m & 0 \\ 0 & U \end{bmatrix} + V^{-1}\tilde{S}_1 V - I \right) \\
&= \begin{bmatrix} I_{m/\varepsilon} & 0 \\ 0 & I_{n-m} \end{bmatrix} \left(\begin{bmatrix} 0 & 0 \\ 0 & U - I_{n-m} \end{bmatrix} + \varepsilon V^{-1}\tilde{S}_1 V \right)
\end{aligned}$$

In the limit $\varepsilon \rightarrow 0$, the top m rows have rank m , since \tilde{S}_1 is full rank (hyperbolicity of the return map $DP_0(p_0)$ asserted in the hypotheses). The bottom $n - m$ rows evaluate to $U - I_{n-m}$; since U has no unity eigenvalues, $U - I_{n-m}$ is also full rank. For $\varepsilon > 0$, the argument is unchanged for the first m rows. For the bottom rows, the entries of $U - I_{n-m}$ dominate those of $\varepsilon V^{-1}\tilde{S}_1 V$ for sufficiently small ε , and so by continuity of eigenvalue with matrix entries, the right-hand side is full rank. Thus, $D_p\zeta$ is full rank, and using the IFT, we know there is a family of fixed points p_ε for P_ε , and $p_\varepsilon = p_0 + \mathcal{O}(\varepsilon)$.

As shown in step (e) in the proof of Theorem (ii), we have $DQ_\varepsilon(p_\varepsilon) = DQ_0(p_0) + \mathcal{O}(\varepsilon^2)$, and we showed in the steps leading to (17) that $DR(Q_\varepsilon(p_0)) = DR(p_0) + \mathcal{O}(\varepsilon^2)$. Similar to those steps, we can show that $DR(Q_\varepsilon(p_\varepsilon)) = DR(p_0) + \mathcal{O}(\varepsilon^2)$. Putting these together,

$$\begin{aligned}
DP_\varepsilon(p_\varepsilon) &= DR(Q_\varepsilon(p_\varepsilon)) DQ_\varepsilon(p_\varepsilon) \\
&= (DR(p_0) + \mathcal{O}(\varepsilon^2)) (DQ_0(p_0) + \mathcal{O}(\varepsilon^2)) \\
&= DP_0(p_0) + \mathcal{O}(\varepsilon^2)
\end{aligned} \tag{18}$$

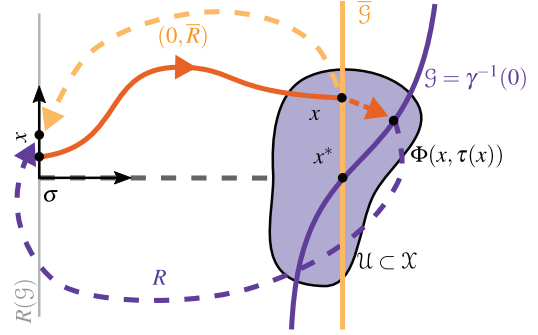


Fig. 1. We define a class of hybrid averageable systems (Theorem 3) with a single domain, fast (σ) and slow (x) coordinates, with general conditions on the flow (dark orange), and requirements on fixed points of the flow and the reset. The calculations in Theorem 3 show how to construct a new hybrid system with constant flow time (yellow, guard $\bar{\mathcal{G}} := \{T\} \times \mathcal{X}$) for any hybrid system with variable flow time (purple, guard $\mathcal{G} = \gamma^{-1}(0)$) by augmenting with a flow-to-reset map.

Following step (f) in the proof of Theorem 1(ii), we conclude the desired result. \square

2.3. Hybrid systems (event-based reset)

Hybrid systems (see Figure 1) arising in legged locomotion and other fields often encounter a discrete reset at a state-dependent “event,” unlike the fixed flow time we assumed in the previous section. The event is usually described as the intersection of the continuous flow with a guard surface, \mathcal{G} , which triggers a discrete reset of the system state. The time elapsed between these events generally varies with initial condition.

In this section we show that the variable event time can be incorporated in a modified reset, effectively reducing this more general case to the switching case, enabling the application and generalization of Theorem 2.

Theorem 3 (Hybrid averaging theorem). *Given the “original” hybrid system*

$$\begin{aligned}
\dot{x} &= \varepsilon f(x, \sigma, \varepsilon), & \dot{\sigma} &= 1 \\
\gamma(x, \sigma) &= 0 & \implies & x_+ = R(x, \sigma)
\end{aligned} \tag{19}$$

and “averaged” switching system

$$\begin{aligned}
\dot{y} &= \varepsilon \bar{f}(y), & \dot{\sigma} &= 1, \\
\sigma &= T & \implies & y_+ = \bar{R}(y)
\end{aligned} \tag{20}$$

where \bar{R} is constructed from R as defined in the proof (23), we assert the following hypotheses on (19)–(20).

- (i) Assuming $D_\sigma \gamma = 1$,⁷ the guard set satisfies $D_x \gamma = \mathcal{O}(\varepsilon)$.
- (ii) The C^r (for $r \geq 2$) reset R (allowed to vary with ε) satisfies: (a) $D_x R(x, \sigma) = S_0 + \varepsilon S_1(x, \sigma, \varepsilon)$ (with constant S_0); (b) S_0 is invertible, and its unity eigenvalues have diagonal Jordan blocks.

(iii) There is a point p_0 and $T > 0$, such that: (a) p_0 is an equilibrium of \bar{f} ; (b) $R(p_0, T) = p_0$; (c) $\gamma(p_0, T) = 0$; and (d) the matrix $S_0 + \varepsilon(\mathbf{U} + \mathbf{V})$, where $\varepsilon\mathbf{U} := \varepsilon S_1(x, T, \varepsilon) - D_\sigma R \cdot D_x \gamma$, $\mathbf{V} := TD\bar{f}$ is hyperbolic at p_0, T .

If conditions (i)–(iii) hold, then there exists $\varepsilon_0 > 0$ such that, for all $0 < \varepsilon \leq \varepsilon_0$, Equation (19) possesses a unique hyperbolic periodic orbit, of the same stability type as p_0 .

Proof. We first provide a construction that enables us to locally transform a system with variable flow time (19), to a system with constant flow time that has equivalent⁸ Poincaré (i.e. flow-and-reset) dynamics. Let $\Phi(x, \sigma)$ denote the maximal flow associated with the continuous dynamics of (19) from the initial condition $(x, \sigma = T)$.⁹ Since $\dot{\sigma} \equiv 1$, $\pi_\sigma \Phi(x, \sigma) = T + \sigma$. Any initial condition $(x, 0)$ impacts the guard as

$$\gamma \circ \Phi(x, \sigma) = 0 \quad (21)$$

where σ may be negative. Applying the IFT (Hirsch et al., 1974, Appendix IV) (justified since $D_\sigma \gamma \circ \Phi \neq 0$) to (21) with respect to t at test point $(x, 0)$ yields a C^1 time-to-event map $\tau : \mathcal{U} \rightarrow \mathbb{R}$ where $\mathcal{U} \subset \mathcal{X}$ is a neighborhood of x (Hirsch et al., 1974, Ch. 11, Section 2) such that $\gamma \circ \Phi(x, \tau(x)) \equiv 0$. Note that the image of τ includes negative times. The derivative (i.e. gradient) of τ can be computed at $(x, 0)$ by differentiating (21) with respect to x (recall that $D_x \Phi(x, 0) = \begin{bmatrix} I \\ 0 \end{bmatrix}$)

$$D\gamma \cdot (D_x \Phi + D_\sigma \Phi \cdot D\tau) = 0 \implies D\tau = \frac{-D_x \gamma}{\varepsilon D_x \gamma \cdot f + 1} \quad (22)$$

since we assumed $D_\sigma \gamma = 1$ without loss of generality. Define the time- T -flow equivalent reset $\bar{R} : \pi_x \mathcal{U} \rightarrow \mathcal{X}$ by

$$\bar{R}(x) := R \circ \Phi(x, \tau(x)) \quad (23)$$

Differentiating with respect to x using chain rule, and substituting using (22) we compute

$$\begin{aligned} D_x \bar{R}(x) &= DR \cdot (D_x \Phi(x, 0) + D_\sigma \Phi \cdot D\tau) \\ &\stackrel{(22)}{=} DR \cdot \left(\begin{bmatrix} I \\ 0 \end{bmatrix} - \frac{1}{\varepsilon D_x \gamma \cdot f + 1} \begin{bmatrix} \varepsilon f \\ 1 \end{bmatrix} D_x \gamma \right) \\ &= D_x R - D_\sigma R \cdot D_x \gamma + \mathcal{O}(\varepsilon^2) \end{aligned} \quad (24)$$

using the hypothesis that $D_x \gamma = \mathcal{O}(\varepsilon)$, and where σ is evaluated at T on the right-hand side.

Let Φ_x now denote the flow of the continuous dynamics of (19) starting from initial condition $(x, \sigma = 0)$. Consider the switching system

$$\dot{x} = \varepsilon f(x, \sigma, \varepsilon), \quad \dot{\sigma} = 1, \quad \sigma = T \implies x \mapsto \bar{R}(x) \quad (25)$$

and its flow-and-reset return map

$$\bar{R} \circ \Phi_x(x, T) \stackrel{(23)}{=} R \circ \Phi(\Phi_x(x, T), \tau \circ \Phi_x(x, T))$$

which corresponds exactly to the return map for (19). In addition, note that $D_x \bar{R} = S_0 + \varepsilon\mathbf{U}$, and that the averaged return map for (20) would be

$$\begin{aligned} D\bar{P}(p_0) &= D\bar{R}(p_0)(I + \varepsilon TD\bar{f}) + \mathcal{O}(\varepsilon^2) \\ &=: S_0 + \varepsilon(\mathbf{U} + \mathbf{V}) + \mathcal{O}(\varepsilon^2) \end{aligned} \quad (26)$$

With the hyperbolicity of $D\bar{P}(p_0)$, all of the conditions of Theorem 2 are satisfied by the systems (25) and (20), and upon its application, we obtain the desired result. \square

Remark 2 (Relation to smoothing). Hybrid systems of the form (19) satisfying the conditions of Theorem 3 (henceforth referred to as “averageable” hybrid systems in this paper) are *smoothable* in the sense that they satisfy the hypotheses of (Burden et al., 2015, Theorem 3). Since that result gives a conjugacy to a classical (non-hybrid) vector field and since the smoothing does not affect the ε -dependence of the vector field, it is unsurprising that we are able to extend classical averaging theory to the present hybrid setting. The contribution in this paper is the provision of a constructive, in fact computational (e.g. Section 4.1), method useful for stability analysis of hybrid systems.

Remark 3 (Lower and upper bounds on ε). The conclusion of the preceding lemma is formally valid only for $\varepsilon > 0$ sufficiently small. However, it may be possible in practice to obtain lower or upper bounds on the allowable range for ε .

1. As we have invoked IFT in the proof of Theorem 1, it is straightforward (if tedious) to bound the size of the neighborhood in which (2) has a periodic orbit as in (Abraham et al., 1988, Supplement 2.5A). Alternatively, singular perturbation methods (Tsatsos, 2006) may provide lower bounds on values of ε that ensure that the conclusions of Theorem 1 hold.
2. An obstruction to enlarging the upper bound on ε appears in our example in Section 4.1: the quotient (41) is only valid when $\dot{x}_1 > 0$, which is violated when $\varepsilon > \omega$.

2.4. Symmetry-factored hybrid averaging

Theorem 3 applies to systems with a single continuous flow (“mode” in hybrid systems terminology (Burden et al., 2015)) punctuated by discrete reset events, as modeled in (19). We are able to use this result to demonstrate stability of a “monoped” in the upcoming Section 4.1. We develop two small extensions to the theoretical result in the following two subsections that allow the result to be applicable in a broader class of “biped” systems that we detail below.

The sagittal plane vertical hopper model we present in Section 3 can have four physical modes (resulting from none, one of the two, or both legs in stance), and Figure 2 suggests how the focus only on in-phase or anti-phase limit cycles leads to a formal reduction to the “single mode with reset” hybrid system (Theorem 3). For the in-phase case

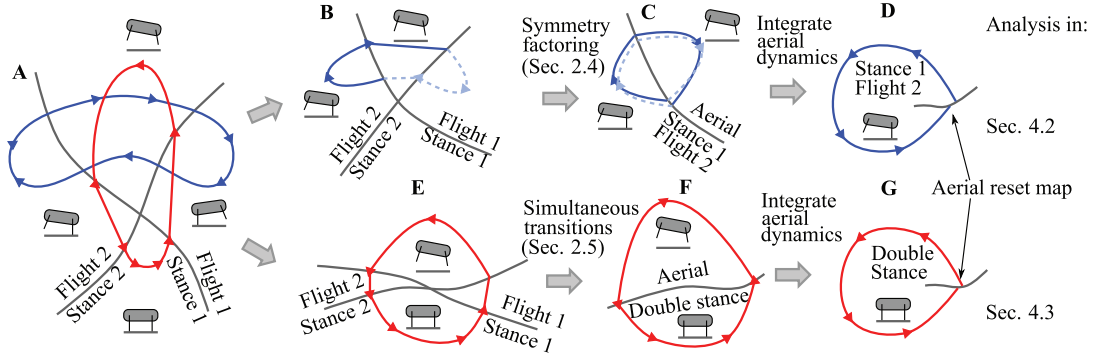


Fig. 2. Depiction of the two kinds of hybrid dynamical limit cycles analyzed in this paper. In the full (visualized as two-dimensional) product domain, there are four possible modes corresponding to each of the two legs being in flight or stance. We (locally) analyze two limit cycles (A): one with alternating stances interspersed with aerial phases (blue), and one with “short” single stance periods. In the former case, we use symmetry (Section 2.4) to factor the return map into two iterations of a “half return map” (27) (B, C), integrate the trivial aerial dynamics, and obtain a single-mode hybrid system (D). In the latter case, we assume that active toe extension control (Section 2.5) can be used to eliminate the short single-stance periods and enforce simultaneous transition between aerial and double stance modes (E, F), integrate the trivial aerial dynamics, and recover another single-mode hybrid system (G). In Section 4.2 and the “weakly coupled hoppers” section in De and Koditschek (2018) we analyze a limit cycle of form D, and in Section 4.3, and the “strongly coupled hoppers” (De and Koditschek, 2018) we analyze a limit cycle of form G.

(bottom row of Figure 2) the limit cycle of interest passes through only two modes (double support and flight). In Section 2.5, we observe that our control affordance (each leg of the abstract “machine” analyzed here, and indeed the physical machine to be analyzed in the companion paper (De and Koditschek, 2018), has two independently actuated DOFs) allows us to force operation into this regime where integrating the aerial dynamics reduces the flight mode to a mere factor of a single mode reset map (as we show in the single-leg example of Section 4.1). However, for the anti-phase case (top row of Figure 2), the limit cycle of interest passes through three modes and even after replacing the flight flow with its integrated reset map, we must still extend the result in Theorem 2 to a class of hybrid systems with two continuous modes. We achieve this extension by imposing a symmetry condition on the dynamics of the two alternating single-stance modes in order to specialize the notion of a standard *hybrid dynamical system* as defined in (Burden et al., 2015, Definition 1), as follows.

Corollary 1. *Given a tuple $\tilde{H} = (\mathcal{X}, \tilde{F}, \tilde{\mathcal{G}}, \tilde{R}, K)$ such that:*

- (i) $(\mathcal{X}, \tilde{F}, \tilde{\mathcal{G}}, \tilde{R})$ is a hybrid dynamical system as defined in (Burden et al., 2015, Definition 1) with two modes in the same domain \mathcal{X} , i.e. index set $J = \{1, 2\} \approx \mathbb{Z}_2$ (we use $\tilde{\cdot}$ to make explicit that these elements are disjoint unions of domains or maps as per convention);
- (ii) $K : \mathcal{X} \rightarrow \mathcal{X}$ is an involutive symmetry, i.e. $K^2 = \text{id}$;
- (iii) the vector field, guard, and reset respect the symmetry, i.e. (a) $DK \cdot F_{(j+1)} \circ K = F_{(j)}$, (b) $\gamma_{(j+1)} \circ K = \gamma_{(j)}$, and (c) $R_{(j+1)} = K \circ R_{(j)} \circ K$;

a limit cycle of the kind depicted in Figure 2B has a return map that can be factored as

$$\tilde{P} = (P_0)^2, \quad \text{where } P_0 := K \circ R_0 \circ Q_0 \quad (27)$$

Proof. The first condition in (iii) essentially states that $F_{(j)}$ are conjugate through the K ; from this we automatically conclude that

$$K \circ Q_{(j+1)} = Q_{(j)} \circ K \quad (28)$$

where $Q_{(j)}$ is the flow of $F_{(j)}$ until it intersects the guard surface $\gamma_{(j)}$. For a limit cycle of the kind depicted in Figure 2B, the full return map can be factored:

$$\begin{aligned} \tilde{P} &= R_{(1)} \circ Q_{(1)} \circ R_0 \circ Q_0 \\ &= (K \circ R_0 \circ K) \circ Q_{(1)} \circ R_0 \circ Q_0 \\ &\stackrel{(28)}{=} K \circ R_0 \circ (Q_0 \circ K) \circ R_0 \circ Q_0 \\ &= (P_0)^2. \end{aligned}$$

□

In (27), P_0 is a “half return map.” It is clear from Corollary 1 that the stability properties of the limit cycle are fully described by the half return map. Consider the single-mode hybrid system, $H_{(1)} = (\mathcal{X}_{(1)}, F_{(1)}, \mathcal{G}_{(1)}, K \circ R_{(1)})$. The return map of $H_{(1)}$ is simply $P_{(1)}$ for all limit cycles of the kind shown in Figure 2B.

Thus, the symmetry properties in Corollary 1(iii) allow us to analyze the single-mode system $H_{(1)}$ and make conclusions about limiting behavior of \tilde{H} . Accordingly, suppressing the single-mode subscript label, we return to the specialized structure of systems compatible with Theorem 3 and consider the tuple $H = (\mathcal{X}, F, \mathcal{G}, R, y^*)$, where $\mathcal{X} := \mathcal{X}_{(1)}$, $F := F_{(1)}$, $\mathcal{G} := \mathcal{G}_{(1)}$, $R := K \circ R_{(1)}$ (again, we emphasize that we have dropped the subscripts since we need only analyze behavior in the first mode), and y^* . In the analytical results of Section 4, we apply Theorem 2 or Theorem

3 for our stability analyses in Section 4.2 and the “weakly coupled hoppers” section of De and Koditschek (2018).

Remark 4. Note that we have made the following notational changes from (Burden et al., 2015, Definition 1): (a) we prefer an implicit (though non-unique) description of the guard set, i.e. $\gamma_{(j)}$ is any function such that $\mathcal{G}_{(j)} \equiv (\gamma_{(j)})^{-1}(0)$; (b) we use parenthesized subscripts for the index set; and (c) we make use of a (non-unique) implicit representation of the guard, $\gamma_{(j)}(\mathcal{G}_{(j)}) \equiv 0$. Apart from notation, it is important to note that the domain for each continuous mode is the same space, \mathcal{X} , and not separate disjoint domains as in Burden et al. (2015).

Remark 5. Symmetry-factoring has been exploited previously to simplify return map calculations in Altendorfer et al. (2004). In that case, *time-reversal symmetry* of Hamiltonian SLIP within a single stance is utilized to factor a SLIP return map, whereas in this paper, we utilize the symmetric steps of a bipedal gait as in Schmitt and Holmes (2000) in order to factor the full return map that represents a complete stride into a “half-return map” (27) that only contains a single step.¹⁰ More generally, notwithstanding the present-seeming special nature of these factorizations, we suspect that symmetry analysis of this nature will play an important role in many more legged locomotion settings.

2.5. Near-simultaneous transitions

We now consider the in-phase limit cycle depicted in the bottom row of Figure 2. Specifically, as anticipated above, we bring its analysis under the sway of the restricted single-mode framework of Theorems 2–3 by enforcing transitions through the higher codimension guard set intersections where both toe-touching constraints are active.

Assumption 1. *In the limit cycles of type Figure 2E–G, active control of the leg extension is used in the aerial phase to execute simultaneous touchdown and liftoff.*

Since the actuators only have to move the toes (small inertia), this action can, in principle, be made almost devoid of any energy cost.

We provide numerical and empirical justification for this assumption following the introduction of more physically realistic models in the companion paper (De and Koditschek, 2018). In the “near-simultaneous transitions” section of De and Koditschek (2018), we compare traces from simulations with active toe extension control in aerial phase either enabled or disabled from a variety of initial conditions to illustrate how the resulting trajectories become nearly indistinguishable after a few strides. Independently, even without imposing such active control on the physical Minitaur robot, the relative frequency of single stance in empirical pronking is low, 6.31% when reflexively pronking in-place (with modified body inertia) and 6.65% when pronking with feedback-stabilized body pitch as shown in plots in De and Koditschek (2018), lending support to our “simultaneous transition” assumption for the

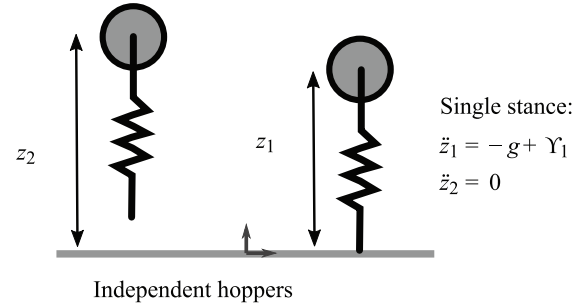


Fig. 3. Two decoupled unit mass vertical hoppers, shown here in a single-stance mode.

pronking analysis (Section 2.5). It is worth noting in passing that these empirical observations, revealing as they do the rarity (even absent active control) of single stance in pronking, lend further support to the suggestion emerging from the analysis of Burden et al. (2016) (motivated by the prevalence of virtual bipedal and monopedal gaits in biology) that such high codimension transitions might, themselves, be reflexively attracting.

3. Model task: vertical hopping

The application domain that motivated the preceding theoretical developments is legged locomotion on land. A well-known model for running is that of a mass suspended on a massless leg by a (physical or virtual) spring (Blickhan and Full, 1993; Geyer et al., 2006). We begin here by considering one (29) or multiple (depicted in Figure 3) vertically constrained legs: a useful model for investigating in-place hopping, bounding (two legs hopping out of phase), and pronking (two legs hopping in phase).

Apart from the utilitarian interest of this regime (where, as we will show in Section 4, it is straightforward to command both in-phase pronking and anti-phase bounding) the effectively decoupled dynamics greatly simplifies the analysis, easing the introduction of notation and permitting simpler stability proofs (that are, nevertheless, strongly evocative of the subsequent reflex stabilized regimes to be analyzed in the companion paper (De and Koditschek, 2018)).

3.1. Equations of motion

Consider a physical plant with a pair of vertically constrained masses (of unit mass), suspended by massless legs with nominal extension $\rho \in \mathbb{R}_+$. The configuration variables of interest are physical heights of the masses, $z_i \in \mathbb{R}_+$.

We obtain two modes, stance and flight, based on whether the height is less than the nominal leg extension (as formalized below in (29)). The equations of motion for the two

hoppers (indexed by $i \in \mathcal{J} := \{1, 2\}$) are

$$\ddot{z}_i = \begin{cases} -g + \Upsilon_i & z_i < \rho \\ -g & \text{otherwise} \end{cases} \quad (29)$$

where Υ_i is the shank extension force generated by leg i . We discuss scaling the controller parameters in relation to the morphological parameters more in De and Koditschek (2018), but for this paper we assume that the shank extension controller compensates for the known dynamical parameters as

$$\Upsilon_i := g + u_i \quad (30)$$

where u_i is the parameter-agnostic “template controller” signal that we define below in (31).

3.2. Model space description

In this section we introduce our preferred coordinates for analysis, and show the results of transforming the vertical hopper pair’s decoupled equations of motion (29). We also introduce the template controllers used in this paper for, first, height regulation in single-legged vertical hopping and, then, coordination control in two-legged vertical hopping.

3.2.1. Vertical hopper control. We set the template vertical hopper controller in stance to have a physical (Blickhan and Full, 1993) or virtual (Kenneally et al., 2016) spring-like force, together with a nonlinearity $v_i(\vec{s})$ (comprising damping as well as active inputs, see (37)) that affects asymptotic stability:

$$u_i := \omega^2(\rho - z_i) + \varepsilon v_i(\vec{s}) \quad (31)$$

where $\vec{s} = (z_1, z_2, \dot{z}_1, \dot{z}_2)$ is the full state vector of the system in Figure 3. Note that there is no gravity compensation term in the template controller above; in (30) just above we declared the relation between (31) and its use as the physical control input in the various plant models in this paper (such as Υ_i in (29)).

3.2.2. Energy-phase coordinates. We write the physical vertical (position and velocity) coordinates in their phase canonical form, $p : \mathbb{R}^2 \rightarrow \mathbb{R}^2$,

$$p(z_i, \dot{z}_i) := \begin{bmatrix} -\dot{z}_i \\ (\rho - z_i)\omega \end{bmatrix}, \quad (32)$$

where $\omega > 0$ is the stance frequency, and consider the square-root-of-energy coordinate $a_i \in \mathbb{R}_+$,

$$a_i := \begin{cases} \|p(z_i, \dot{z}_i)\| & z_i < \rho \\ \sqrt{2g(z_i - \rho) + \dot{z}_i^2} & \text{otherwise} \end{cases} \quad (33)$$

Note that $m_b a_i^2 / 2$ (in Joules) represents the total mechanical energy of a vertical hopper. However, motivated by the analytical simplicity of the resulting stance dynamics (Sections

4.1 and 4.2), we find it convenient to assume unit mass and work in the square root. Consequently, the units of a_i in (33) are meters per second, and intuitively it captures the vertical speed at liftoff or touchdown. In addition, since both expressions in (33) reduce to the square root of (mass-specific) energy at touchdown, a_i is continuously defined around the cycle. As the reader might anticipate, this quantity derived from the total mechanical energy has slow dynamics in a desirable periodic orbit of a hopper and, indeed, we show this in (41). This makes a_i a good candidate to be one of the “ x ” coordinates of Theorem 3, and indeed we use it in such capacity in Section 4.1.

Also define the corresponding phase, $\psi_i \in \Psi \subset \mathbb{R}$,

$$\psi_i := \begin{cases} \angle p(z_i, \dot{z}_i) & z_i < \rho \\ \frac{a_i - \dot{z}_i}{2a_i} & \text{otherwise} \end{cases} \quad (34)$$

where “ $\angle\theta$ ” refers to the “angle of $\theta \in S^1$,” and the stance phase is the natural completion of the polar coordinate transformation in (33), the flight phase definition is from Klavins et al. (2000), and we refer the reader to Remark 6 again for the implications of the discontinuity in this definition.

Note that around the cycle, ψ_i goes from 0 to π in stance, and from 0 to 1 in flight. Define the “flight frequency,”

$$\omega_f : \mathbb{R}_+ \rightarrow \mathbb{R}_+ : a_i \mapsto g / (2a_i) \quad (35)$$

The abstract phase definition here is inspired by the work of Klavins et al. (2000). However, the process of generating a constant-slope phase coordinate (referred to as a “smoothing” step in Klavins et al. (2000, Section 3.2)) is much more difficult in our case because of the various nonlinearities and coupling forces. We discuss further connections to Klavins et al. (2000) in the Appendix.

Remark 6 (Continuity in maps from physical to model coordinates). All dynamical models considered in this paper fall within the class of self-manipulation hybrid systems (Johnson et al., 2016) and are thus guaranteed to have unique and non-blocking executions. We further show, using the distinct strategies depicted in Figure 2, that they satisfy the requirements of Theorem 3, placing them within the class of “smoothable” hybrid systems (Burden et al., 2015, Theorem 3), so that their executions are also guaranteed to vary continuously with respect to initial conditions and be piecewise smooth. Because our coordinate transformations, e.g. (34) are written for convenience across the distinct modes of the original physical coordinates of the self-manipulation system, they are not formally continuous functions. However, as depicted in Figure 2, both routes to the single mode averageable model set out in Theorem 3 subsume into its formal reset map the erstwhile continuous flows through “uninteresting” (and integrable) modes of the physical coordinates, so that (34) and (36) operate only in a single mode in which they are indeed smooth functions.

3.2.3. Phase differences. For the analyses we present in Section 4 and the analysis section in De and Koditschek (2018), the principal tool we use is single-mode hybrid averaging (Theorem 2–3). The result allows us to make local stability conclusions about hyperbolic hybrid limit cycles, but is only applicable to continuous dynamics with a single “fast” variable (which can be thought of as a phase-like coordinate). In order to express the dynamics of our plant models in terms amenable to application of hybrid averaging, we use our intuition to find appropriate slow “phase difference” coordinates (36). This idea is inspired by Proctor et al. (2010), where differences of phases of identical coupled oscillators are shown to be slow, and a classical averaging application follows.

We introduce the following *local* (by this we mean that δ is a smooth function of the physical states while in a single hybrid mode, but discontinuous across modes¹¹) definition for “phase difference:”

$$\begin{aligned} \delta &:= \tau_1 - \tau_2, \text{ where} & (36) \\ \tau_i &:= \begin{cases} (\psi_i - \pi/2)/\omega & z_i < \rho \\ (\psi_i - 1/2)/\omega_f(a_i) & \text{otherwise} \end{cases} \end{aligned}$$

Note that the coordinates above have the units of time (this is apparent from the definition above, since ψ_i are unitless (34), and ω (31) and ω_f (35) both have units of per second).

3.2.4. Oscillatory energization and phase control. The v_i term in our vertical hopper control (31) contains the various nonlinearities responsible for asymptotic stability and phase control. This includes a lumped viscous friction term (which is assumed to come from unavoidable parasitic sources), as well as terms introduced by feedback:

$$v_i(\vec{s}) := -\beta\dot{z}_i - k_a \cos \psi_i + w_i(\vec{s}) \quad (37)$$

where the second summand in the last equation is an oscillatory energization term (De and Koditschek, 2015b) that can intuitively be thought of as “negative damping,”¹² and the last summand introduces a new feedback phase-control term. The phase controller expressed in the functional form of $w_i(x)$ is discussed in Section 3.3.

3.3. Coordination controllers.

In this paper, we propose two kinds of coordination controllers. First, we introduce a *phase controller*¹³ with phase control gain $k_d \in \mathbb{R}$,

$$w_i(\vec{s}) = (-1)^{i-1} k_d (\dot{z}_1 - \dot{z}_2) \sin \psi_i \quad (38)$$

Looking ahead, setting $k_d > 0$ in Section 4.2 stabilizes an anti-phase limit cycle (the template for a “bounding” gait in the “weakly coupled hoppers” section in De and Koditschek (2018)), whereas setting $k_d < 0$ in Section 4.3 stabilizes a limit cycle entraining the two legs in-phase (the template for

a “pronging” gait in the “strongly coupled hoppers” section in De and Koditschek (2018)).

Second, we introduce an empirically motivated *attitude controller* (only for pronk stabilization) that adds a proportional control term to (38),

$$w_i(\vec{s}) = (-1)^{i-1} (k_p(z_1 - z_2) + k_d(\dot{z}_1 - \dot{z}_2)) \quad (39)$$

for $i \in \mathcal{J}$.

We verify analytically the efficacy of these controllers with respect to the mechanically isolated hoppers of Figure 3 in Section 4. In the companion paper we will show, first, that these stability results persist for a weakly mechanically coupled instance of the hoppers (De and Koditschek, 2018) and, then, turn to a similar but more intricate analysis of what we will term “preflexive” stabilization wherein the influence of two distinct modes of (first, stronger, and then much stronger) mechanical coupling substitutes in place of any feedback control.¹⁴

We remark here that (38) and (39) are both trivial to implement on a physical platform, since the only sensory information required is of the coordinate $z_1 - z_2$, and its derivative. For example, on the physical Minitaur robot of the companion paper (De and Koditschek, 2018) this information can be measured directly through the physical angle ϕ and its derivative.

4. Analytical results

Our stability analyses of the various models and control schemes take the form of systematically working through the checklist of conditions of Theorem 2 or 3.

The generalization to variable flow-time achieved by Theorem 3 (over Theorem 2) allows us to account for variable stance duration caused by the nonlinear forcing (31) and (37) the springy leg is subject to. In Section 4.1, we model in detail the weakly varying (45) stance duration and account for this effect in the linearized return map Jacobian (26). However, just as (Raibert, 1986, Ch. 2) argued, we find in our empirical tests referenced from the table of assumptions in De and Koditschek (2018) that the variation in stance duration of a spring–mass system with weak forcing is negligible. Thus, we enforce a constant stance time assumption (Assumption 2) for Sections 4.2–4.3 to simplify our exposition. Nonetheless, we include the requisite calculations for a variable-flow-time version of the analysis in Section 4.2 in Section 4.2.4 in order to convey to the reader the conceptual simplicity of the computations. We anticipate that Theorem 3 will have great utility in situations where the flow duration varies significantly, such as the “preloaded” leg spring strategies explored in (Raibert et al., 1989, equation (4.6)) for high-speed running.

4.1. Single vertical hopper

To demonstrate the applicability of hybrid averaging to the analysis of physical systems, we first investigate a 1-DOF

hybrid system. We consider one of the two hoppers depicted in Figure 3: a unit mass restricted to travel along its vertical axis with an attached massless leg. We choose this as our first example for two reasons. First, despite its apparent simplicity, it serves as a template for ubiquitous running and hopping behavior in robots and animals (Blickhan and Full, 1993). Variants of this model have been analyzed extensively in the literature, see e.g. Koditschek and Buehler (1991) for an analysis of this 1-DOF restriction of a planar point-mass model whose energizing input is inspired by the empirically successful strategies reported in Raibert (1986). Second, the simplicity of the equations of motion mitigate the intricacies of the hybrid averaging, exposing in particular the synergistic relationship of this method with symmetry, which we discuss further in Section 4.1.1.

Informed by the structure of the averaging results of Section 2, we propose an alternative energization scheme (intuitively similar but physically distinct from Raibert (1986)) and apply Theorem 1 to establish an analogous stability result. The analyses in Koditschek and Buehler (1991) relied on two simplified models that both admitted closed-form return maps (Koditschek and Buehler, 1991, equations (15) and (17)). However, hybrid averaging allows a stability analysis without requiring integrable¹⁵ stance dynamics (e.g. (41)). Recall that even the “simple” 2-DOF SLIP dynamics (Saranli et al., 1998) are non-integrable, hence motivating an analysis tool that drops this requirement.

4.1.1. Continuous dynamics. For the following analysis, we choose (in the language of Theorem 3) the coordinates $\sigma := \psi_1 \in \mathcal{X}_1$ and $x := a_1 \in \mathbb{R}$.

Using the previously declared vertical hopper model in (3.1) and control in (31) and (37), setting $w_i \equiv 0$ (because there is no “other” hopper to coordinate for now) in the system dynamics (29) and (30), we derive the stance (a_1, ψ_1) equations of motion of the hopper as follows.

Define $q := p(z_1, \dot{z}_1)$ from (32). The physical equation of motion in stance (from (29) and (31)) is

$$\ddot{z}_1 = \omega^2(\rho - z_1) + \varepsilon v_1$$

and rewritten in terms of q are

$$\begin{aligned} \dot{q}_1 &= -\dot{z}_1 = \omega^2(z_1 - \rho) - \varepsilon v_1 = -\omega q_2 - \varepsilon v_1 \\ \dot{q}_2 &= -\dot{z}_1 \omega = q_1 \omega \end{aligned} \quad (40)$$

Using (33), $a_1 = \|q\|$, and from the equations above,

$$\begin{aligned} a_1 \dot{a}_1 &= q^T \dot{q} = -\varepsilon v_1 q_1 = -\varepsilon v_1 (a_1 \cos \psi_1) \\ \Rightarrow \dot{a}_1 &= -\varepsilon v_1 \cos \psi_1 \end{aligned}$$

where we used the polar coordinate transformation of q , i.e. $q_1 = a_1 \cos \psi_1$ and $q_2 = a_1 \sin \psi_1$. For the ψ_1 dynamics, note that

$$\begin{aligned} \dot{q}_1 &= -a_1 \sin \psi_1 \dot{\psi}_1 + \dot{a}_1 \cos \psi_1 \\ \dot{q}_2 &= a_1 \cos \psi_1 \dot{\psi}_1 + \dot{a}_1 \sin \psi_1 \end{aligned}$$

and note that $q_1 \dot{q}_2 - q_2 \dot{q}_1 = a_1^2 \dot{\psi}_1$. Then,

$$\begin{aligned} \dot{\psi}_1 &\stackrel{(40)}{=} \frac{1}{a_1^2} (q_1^2 \omega - q_2(-\omega q_2 - \varepsilon v_1)) \\ &= \frac{1}{a_1^2} (\omega^2 (q_1^2 + q_2^2) + \varepsilon v_1 q_2) = \omega + \varepsilon v_1 \sin \psi_1 / a_1 \end{aligned}$$

since $q_1^2 + q_2^2 = a_1^2$.

We observe that for sufficiently small $\varepsilon > 0$, we have $\dot{\psi}_1 > 0$, allowing us to divide \dot{a}_1 by $\dot{\psi}_1$. Now in the language of Theorem 3, $\sigma = \psi_1$, $x = a_1$, and we can write

$$\frac{\partial a_1}{\partial \psi_1} = \frac{-\varepsilon \cos \psi_1 v_1}{\omega + \frac{\varepsilon}{a_1} \sin \psi_1 v_1} \quad (41)$$

where v_1 is as given in (37). Note that the system takes the form of (19). Consider the prospective fixed point for the averaged system,

$$T = \pi, \quad y^* = k_a / \beta \quad (42)$$

where the value of T corresponds to the state having traversed the entire half plane of stance (i.e. the state of liftoff) and the value of y^* (i.e. energy a_1^*) corresponds to the equilibrium energy suggested by the second summand of (37). Using this T for direct integration of the stance vector field (41) from touchdown through to liftoff, we obtain (now, as in (2), letting $y = a_1$),

$$\begin{aligned} \bar{f}(y) &:= \int_0^\pi \frac{f(y, \sigma, 0) d\sigma}{\pi \omega} = - \int_0^\pi \frac{v_1 \cos \psi_1 d\psi_1}{\pi \omega} \\ &= \frac{(k_a - a_1 \beta)}{2\omega}, \end{aligned} \quad (43)$$

which indeed evaluates to 0 at y^* (42), satisfying Theorem 3(iii).

In intuitive terms, we point out that the oscillatory control signal introduced in (37) has the special property that the k_a -term is *odd*¹⁶ in ψ_1 in the first row of (41), whereas it is *even* in ψ_1 in the second row. Consequently, after the averaging step, k_a persists in the averaged a_1 -dynamics (43). In more complex future analysis expanding on these ideas (as discussed in the conclusion), we see that similar odd symmetries (e.g. last row of (53)) are helpful in eliminating coupling interactions.

4.1.2. Guard set. The guard set is defined by the physical liftoff event when the normal force at the toe-ground interface during stance goes to 0, and from (29) and (30), we see that this happens when $u_i = 0$ in (31):

$$\gamma(x, \sigma) := \tan \psi_1 - \frac{\varepsilon(k_a/a_1 - \beta)}{\omega} \quad (44)$$

scaled such that $D_\sigma \gamma = 1$ at $\sigma = T$. In addition, $D_x \gamma = \mathcal{O}(\varepsilon)$, satisfying Theorem 3(i). Lastly, note that $\gamma(y^*, T) = 0$ at the fixed point of the averaged vector field (43), satisfying Theorem 3(iii). In addition, we can calculate

$$D\gamma(y^*, T) = \begin{bmatrix} 1 & \frac{\varepsilon \beta^2}{k_a \omega} \end{bmatrix} \quad (45)$$

We observe that Lemma 1 allows us to apply both x and y coordinates as arguments to γ , since both sets of coordinates coincide at liftoff time.

4.1.3. Reset map. As in De and Koditschek (2015a), the massless in-flight leg is reset to its nominal length, ρ . It follows from (34) that the touchdown phase, ψ_1 is identically zero since $z_1 = \rho$ at the touchdown event. Noting from (34) that $\dot{z}_1 = -a_1$ at touchdown, and recalling that the mechanical energy a_1 is conserved in flight (33), we can solve for a_1 at touchdown, yielding

$$R(x, \sigma) = \sqrt{a_1^2 \cos^2 \psi_1 - 2ga_1 \sin \psi_1 / \omega} \quad (46)$$

$$\implies DR(y^*, T) = [1, g/\omega] \quad (47)$$

where $S_0 := 1$ is constant, satisfying Theorem 3(ii). In addition, $R(y^*, T) = y^*$ from (46), satisfying Theorem 3(iii). Again, we observe that Lemma 1 allows us to apply both x and y coordinates as arguments to R .

4.1.4. Stability test. We can calculate U according to the definition in Theorem 3 to obtain

$$S_0 + \varepsilon U = D_y R - D_\sigma R D_y \gamma \stackrel{(45),(47)}{=} 1 - \frac{\varepsilon g \beta^2}{k_a \omega^2}$$

where the second summand was introduced by the variable flow time. As pointed out in the introduction of Section 4.1, this effect empirically appears to be negligible, likely due to the small magnitude of the second summand. We can also compute V by differentiating (43) to obtain $V = -\frac{\pi\beta}{2\omega}$.

As in (26), using the previous computations, the averaged return map linearization is

$$D\bar{P}(y^*) = 1 - \varepsilon \left(\frac{g\beta^2}{k_a \omega^2} + \frac{\pi\beta}{2\omega} \right),$$

which is stable as well as hyperbolic for small $\varepsilon > 0$. We conclude from Theorem 3 that the (unaveraged) vertical hopper also has a stable fixed point that is ε -close¹⁷ to (42). We present a numerical demonstration of this result in Section 5.1.

4.2. Two vertical hoppers: anti-phase limit cycle (bounding template)

Here we present a local analysis of the anti-phase limit cycle with alternating stances of hoppers 1 and 2, the results of which are borne out in empirical trials in De and Koditschek (2018).

We appeal to Corollary 1 with symmetry (48), and study the half return map with the continuous dynamics $F := F_{(1)}$, where mode “1” we now define as that where hopper 1 is in stance, hopper 2 in flight, and where the reset $R := K \circ R_{(1)}$, where $R_{(1)}$ maps states from liftoff of hopper 1 to touchdown of hopper as depicted in the upper series of sketches in Figure 2.

The full state space thus has four dimensions. The symmetry map (Corollary 1(iii))

$$K : \mathbb{R}^4 \rightarrow \mathbb{R}^4 : (a_{(j)}, \psi_{(j)}) \mapsto (a_{(j+1)}, \psi_{(j+1)}) \quad (48)$$

is helpful in defining the reset maps in Section 4.2 and the “weakly coupled hoppers” section of De and Koditschek (2018).

For this subsection and the next, we enforce the following assumption, whose justification is referenced from the assumptions table in De and Koditschek (2018).

Assumption 2. *The stance duration (resulting from a weakly perturbed spring-mass oscillation) is constant.*

As described in the introduction of Section 4, our empirical trials display more-or-less constant flow time, and we find that the further complication in algebra does not buy any new insight. Still, we include a variable-flow-time version of the return map computation (and stability analysis) that appears in Section 4.2.3 to demonstrate in a tutorial manner how an application of Theorem 3 would proceed.

4.2.1. Continuous dynamics. For the following analysis, we choose the coordinates $\sigma := \psi_1$, and $x := (a_1, a_2, \delta)$, where δ is the phase difference coordinate introduced in Section 3.2.3. The projection of the symmetry map K to these x -coordinates is a linear map defined by the matrix

$$\bar{K} := \begin{bmatrix} 0 & 1 & 0 \\ 1 & 0 & 0 \\ 0 & 0 & -1 \end{bmatrix} \in \mathbb{R}^{3 \times 3} \quad (49)$$

The continuous dynamics (29) can be rewritten in the coordinates defined in (33)–(34), as we have already shown for the stance leg in Section 4.1 in (41).

For the leg in flight ($\dot{a}_2, \dot{\psi}_2$), from the second row of (33),

$$\frac{d}{dt} \frac{a_2^2}{2} = a_2 \dot{a}_2 = g z_2 + \dot{z}_2 \dot{z}_2 = \dot{z}_2 (\dot{z}_2 + g) \stackrel{(29)}{=} 0 \quad (50)$$

and from the second row of (34),

$$\dot{\psi}_2 \stackrel{(50)}{=} -\frac{\dot{z}_2}{2a_2} \stackrel{(29)}{=} \frac{g}{2a_2} \stackrel{(35)}{=} \omega_f(a_2)$$

Putting it all together,

$$\begin{aligned} \dot{a}_1 &= -\varepsilon \cos \psi_1 v_1, & \dot{a}_2 &= 0, \\ \dot{\psi}_1 &= \omega + \frac{\varepsilon}{a_1} \sin \psi_1 v_1, & \dot{\psi}_2 &= \omega_f(a_2) \end{aligned} \quad (51)$$

where the ε parameter appears in these positions due to our choice of ε magnitude nonlinearity in the hopper control (31) so as to depend upon the anti-phase stabilizing version ($k_d > 0$) of the phase coordination term w_1 defined in (38).

Using the phase difference coordinate δ from (36) (note that hopper 1 is in stance and hopper 2 is in flight for the analysis in this subsection), we note that

$$\frac{d}{dt} \delta = \frac{\varepsilon}{\omega a_1} \sin \psi_1 v_1 \quad (52)$$

i.e. by inspection, the presence of the “small” parameter, the factor ε in (52), reveals that the chosen phase difference coordinate is “slow” ($\mathcal{O}(\varepsilon)$ dynamics). The continuous dynamics in these coordinates are

$$\begin{aligned} \dot{\sigma} &= \omega + \varepsilon \frac{\sin \psi_1 v_1}{a_1} \\ \dot{x} &= \varepsilon \begin{bmatrix} -\cos \psi_1 v_1 \\ 0 \\ \frac{\sin \psi_1 v_1}{\omega a_1} \end{bmatrix} \end{aligned} \quad (53)$$

Consider the prospective anti-phase fixed point,

$$T = \pi, \quad y^* = [\tilde{k}_a/\tilde{\beta}, \tilde{k}_a/\tilde{\beta}, 0]^T \quad (54)$$

where

$$\tilde{k}_a := k_a + \frac{gk_d}{2\omega}, \quad \tilde{\beta} := \beta - \frac{4k_d}{3\pi} \quad (55)$$

Although the last entry of (54) is zero, we emphasize that this denotes an “anti-phase” limit cycle: observe in (36) that when hopper 2 attains apex, $\tau_1 = 1/2$, then $\delta = 0$ implies that, simultaneously, the hopper must be experiencing its “bottom” (most compressed) event.

In addition, note from (54) that the k_d gain introduced through our phase controller (38) moves the first two components, of the equilibrium, y^* , $a_1^* = a_2^* = \tilde{k}_a/\tilde{\beta}$, smoothly as a function of that controller gain k_d . The limiting $k_d = 0$ case recovers the isolated vertical hopper equilibrium point (42). Direct integration of (53), using (38) with $k_d > 0$, yields

$$\bar{f}(y) := \int_0^\pi \frac{dy}{d\sigma} d\sigma = \frac{1}{2\omega} \begin{bmatrix} \tilde{k}_a - a_1 \tilde{\beta} \\ 0 \\ -\frac{gk_d}{\omega^2 a_1} \delta \end{bmatrix} \quad (56)$$

which evaluates to 0 at y^* , satisfying Theorem 2(ii). Moreover, anticipating its use in (63), we can calculate the Jacobian as

$$D\bar{f}(y) = \begin{bmatrix} -\frac{\tilde{\beta}}{2\omega} & 0 & 0 \\ 0 & 0 & 0 \\ \frac{gk_d}{2\omega^3 a_1^2} & 0 & -\frac{gk_d}{2\omega^3 a_1} \end{bmatrix} \quad (57)$$

4.2.2. Reset. The touchdown condition is triggered by the event that hopper 2 touches down, or $\psi_2 - 1$ (34) crosses zero. Thus, using K as defined in (48), $\pi_1 \circ K \circ R_{(1)} \equiv 0$, satisfying Theorem 2(i), where $R_{(1)}$ maps the state from liftoff of hopper 1 to touchdown of hopper 2 (as in Corollary 1), and is obtained by integrating the trivial aerial dynamics, as detailed below.

Note that the a_i are defined continuously through modes (33), and the a_i are unchanged by ballistic flight.

Define t_{LO} as the liftoff time (when hopper 1 is in stance, hopper 2 is in flight) and t_{TD} as the touchdown time (when hopper 1 is in flight, hopper 2 is in stance). In this reset

calculation, to avoid confusion, we will be explicit about which row of (34) is used in each appearance of ψ_i , e.g. $\psi_f^{(2)} = (a_2 - \dot{z}_2)/(2a_2)$.

First, we integrate the aerial dynamics. Note that the time of flight is t_f is given by

$$\psi_f^{(2)}(t_{LO}) + \omega_f(a_2) t_f = 1 \implies t_f = \frac{1 - \psi_f^{(2)}(t_{LO})}{\omega_f(a_2)}$$

Using this in $\psi_f^{(1)}(t_{TD}) = \psi_f^{(1)}(t_{LO}) + \omega_f(a_1) t_f$, and noting from (34) that $\psi_f^{(1)}(t_{LO}) = 0$, we obtain the flight map

$$\psi_f^{(1)}(t_{TD}) = \frac{\omega_f(a_1)}{\omega_f(a_2)} (1 - \psi_f^{(2)}(t_{LO})) \quad (58)$$

Now we must express the above in terms of δ . Using the appropriate patches at t_{LO} and t_{TD} ,

$$\begin{aligned} \delta(t_{LO}) &= \frac{\psi_v^{(1)}(t_{LO}) - \pi/2}{\omega} - \frac{\psi_f^{(2)}(t_{LO}) - 1/2}{\omega_f(a_2)} \\ \delta(t_{TD}) &= \frac{\psi_f^{(1)}(t_{TD}) - 1/2}{\omega_f(a_1)} - \frac{\psi_v^{(2)}(t_{TD}) - \pi/2}{\omega} \end{aligned} \quad (59)$$

Per our constant flow-time assumption (Assumption 2), we know that $\psi_v^{(1)}(t_{LO}) = \pi$, and combining with (59),

$$\delta(t_{LO}) = \frac{\pi}{2\omega} - \frac{\psi_f^{(2)}(t_{LO}) - 1/2}{\omega_f(a_2)} \quad (60)$$

Since the leg touches down at its nominal extension, by (34), $\psi_v^{(2)}(t_{TD}) = 0$, and combining with (59),

$$\begin{aligned} \delta(t_{TD}) &= \frac{\psi_f^{(1)}(t_{TD}) - 1/2}{\omega_f(a_1)} + \frac{\pi}{2\omega} \\ &\stackrel{(60)}{=} \frac{\psi_f^{(1)}(t_{TD}) - 1/2}{\omega_f(a_1)} + \delta(t_{LO}) + \frac{\psi_f^{(2)}(t_{LO}) - 1/2}{\omega_f(a_2)} \end{aligned} \quad (61)$$

Substituting (58) into the above,

$$\begin{aligned} \delta(t_{TD}) &= \delta(t_{LO}) - \frac{1}{2\omega_f(a_2)} - \frac{1}{2\omega_f(a_1)} + \frac{1}{\omega_f(a_2)} \\ &= \delta(t_{LO}) + \frac{1}{2\omega_f(a_2)} - \frac{1}{2\omega_f(a_1)} = \delta + \frac{(a_2 - a_1)}{g} \end{aligned}$$

All together, the slow-coordinate reset is

$$\begin{aligned} R(a_1, a_2, \delta) &= \pi_2 \circ K \circ \begin{bmatrix} \psi_1 \\ a_1 \\ a_2 \\ \delta + (a_2 - a_1)/g \end{bmatrix} \\ &= \bar{K} \begin{bmatrix} a_1, & a_2, & \delta + \frac{(a_2 - a_1)}{g} \end{bmatrix}^T \end{aligned} \quad (62)$$

From the above, we observe that DR has a constant $\mathcal{O}(1)$ part, satisfying Theorem 2(i).

4.2.3. *Application of switching averaging.* Using (49), (57), and (62) and evaluating at (54), we obtain the averaged return map

$$\begin{aligned} D\bar{P} &:= DR \cdot (I + \varepsilon\pi D\bar{f}) \\ &= \left[\begin{array}{cc|c} 0 & 1 & 0 \\ \zeta_1 & 0 & 0 \\ \hline \frac{\zeta_1}{g} & -\frac{1}{g} & -1 + \frac{\varepsilon g k_d \beta}{2k_a \omega^3} \end{array} \right] \end{aligned} \quad (63)$$

where

$$\zeta_1 := 1 - \frac{\varepsilon\beta}{2\omega} \quad (64)$$

only depends on constant parameters. The block lower triangular $D\bar{P}$ has eigenvalues $\pm j\sqrt{\zeta_1}$ from the upper left block (the upper block has complex conjugates hence the determinant is their magnitude squared), and $-1 + \frac{\varepsilon g k_d \beta}{2k_a \omega^3}$ from the scalar lower right block, which is within the unit circle for small $\varepsilon > 0$.

This computation reveals a condition on allowable parameter values; in (38), k_d must be small enough such that $\tilde{\beta} > 0$. Assuming our gains are set appropriately, for small $\varepsilon > 0$, $|\zeta_1| < 1$, and also the other eigenvalues are within the unit circle since their product is ζ_1 , and the averaged return map is stable. In addition, the return map is hyperbolic, and applying Theorem 2, we conclude that the pair of independent hoppers has a stable anti-phase limit cycle ε close to (54).

4.2.4. Variable flow-time (event-based reset) analysis.

This section contains a ‘‘tutorial’’ description of how Theorem 3 can be applied (without requiring Assumption 2) to the bounding analysis of Section 4.2. We point out specific departures from the constant-flow-time version of the analysis below, and end by juxtaposing the return map linearization (66) against its constant-flow-time counterpart (63).

Guard set First, the guard set is defined by the ‘‘normal reaction crossing zero’’ event as in (44).

Reset Next, the reset map is modified in two of its entries.

1. Note that a_1 is constant through flight, but we need to convert its stance coordinates at the time of liftoff (depending on when the guard surface (44) is intersected) to flight coordinates. Thus, the a_1 reset is replaced instead by (46) (see (65) below).
2. In addition, the phase difference reset calculation is modified. We replace (60) with the guard (44), and obtain

$$\delta(t_{LO}) = \frac{\tan^{-1}(\varepsilon k_a / (\omega a_1) - \beta)}{2\omega} - \frac{\psi_f^{(2)}(t_{LO}) - 1/2}{\omega_f(a_2)}$$

Using this together with (61), we obtain

$$\begin{aligned} \delta(t_{TD}) &= \delta(t_{LO}) + \frac{1}{2\omega_f(a_2)} - \frac{1}{2\omega_f(a_1)} \\ &\quad + \frac{\pi - \tan^{-1}(\varepsilon k_a / (\omega a_1) - \beta)}{2\omega} \end{aligned}$$

Putting these together, and applying the symmetry operation (48)

$$R_{(1)}(x, \psi_1) = \left[\begin{array}{c} \sqrt{a_1^2 \cos^2 \psi_1 - 2ga_1 \sin \psi_1 / \omega} \\ a_2 \\ \delta + \frac{(a_2 - a_1)}{g} + \frac{\pi - \tan^{-1}(\varepsilon k_a / (\omega a_1) - \beta)}{2\omega} \end{array} \right] \quad (65)$$

Note from (54) that

$$R \left(\begin{bmatrix} \tilde{k}_a / \tilde{\beta} \\ \tilde{k}_a / \tilde{\beta} \\ 0 \end{bmatrix} \right) = \bar{K} \begin{bmatrix} \tilde{k}_a / \tilde{\beta} \\ \tilde{k}_a / \tilde{\beta} \\ 0 \end{bmatrix} = \begin{bmatrix} \tilde{k}_a / \tilde{\beta} \\ \tilde{k}_a / \tilde{\beta} \\ 0 \end{bmatrix}$$

satisfying $\bar{R}(y^*) = y^*$ in Theorem 3(iii). Next, we use (24) to find $D\bar{R}$. Using the guard (44) and the reset (65), and evaluating at the fixed point (54), we obtain

$$D\bar{R}_{(1)}(y^*) = \begin{bmatrix} 1 - \frac{\varepsilon g \beta^2}{k_a \omega} & 0 & 0 \\ 0 & 1 & 0 \\ -1/g & 1/g & 1 \end{bmatrix}$$

which has a constant $\mathcal{O}(1)$ part. We also note the similarity between the top left entry and Section 4.1. Repeating the steps in Section 4.2.3, we obtain the averaged return map

$$D\bar{P} = \left[\begin{array}{cc|c} 0 & 1 & 0 \\ \zeta_1 - \frac{\varepsilon g \beta^2}{k_a \omega} & 0 & 0 \\ \hline \frac{\zeta_1}{g} & -\frac{1}{g} & -1 + \frac{\varepsilon g k_d \beta}{2k_a \omega^3} \end{array} \right] \quad (66)$$

Note that the eigenstructure of this matrix is similar to its constant-flow-time counterpart (63). In fact, since $\zeta_1 - \frac{\varepsilon g \beta^2}{k_a \omega} < \zeta < 1$ for small ε , the eigenvalues for the block lower triangular matrix above are within the unit circle.

4.3. Two vertical hoppers: in-phase limit cycle (pronking template)

In this section we show that phase control (38) (albeit now with $k_d < 0$) can be applied to the same independent hoppers model as in the previous subsection (Figure 3) but now used to stabilize a different limit cycle.

As depicted in the lower succession of sketches in Figure 2, we think of this limit cycle as having a single continuous mode (double stance) followed by a reset (aerial phase), assuming simultaneous transitions as discussed in Section 2.5. With this assumption in force, we now show, in counterpoint to the previous section (where the introduction of a symmetry operator (48) achieves a re-factorization of the three physical modes depicted in Figure 2B into the ‘‘half-stride’’ paired modes depicted in Figure 2C), how

these different hybrid dynamics can directly be modeled as executions of a single-mode averageable hybrid system.

In this instance, we again use the switching theorem (Theorem 2) and ignore the small variation in the flow duration.

4.3.1. Continuous dynamics. As in (51), but this time, since both legs are in stance, for $i \in \mathcal{J}$ we get (29) for both legs. Use the phase difference δ in the double-stance patch from (36), and note that

$$\begin{aligned} \frac{d}{dt}\delta &= \frac{\varepsilon}{\omega^2} \left(\frac{v_2 \sin(\omega\delta - \psi_1)}{a_2} + \frac{v_1 \sin \psi_1}{a_1} \right) \\ &=: f_\delta(x) \end{aligned} \quad (67)$$

i.e. the phase difference is “slow” analogously to its counterpart (52) in the anti-phase limit cycle analysis of the preceding Section 4.2.1. Once again as in Section 4.2, we use the coordinates, $\sigma = \psi_1 + \pi/2$ and $x := (a_1, a_2, \delta)$, and see that

$$\begin{aligned} \dot{\sigma} &= \omega + \frac{\varepsilon}{a_1} \sin \psi_1 v_1 \\ \dot{x} &= \varepsilon \begin{bmatrix} -\cos \psi_1 v_1 \\ -\cos(\omega\delta - \psi_1) v_2 \\ f_\delta(x) \end{bmatrix} \end{aligned} \quad (68)$$

where $f_\delta(x)$ is defined in (67). Recall we are using the same phase controller (38) as in Section 4.2, but now with $k_d < 0$. Introducing the prospective in-phase fixed point,

$$T = \pi, \quad y^* = [k_a/\beta, k_a/\beta, 0]^T \quad (69)$$

we point out here that the equilibrium phase difference above is very different from that in (54) despite the visual similarity, due to the different definition of δ (which is, as before in Section 4.2, local). Recall again that in Section 4.2.1 we considered hopper 1 to be in stance and hopper 2 to be in flight, whereas now both hoppers are assumed to be in stance. Consequently, Equation (36) shows that δ is zero if and only if both hoppers attain “bottom” simultaneously.

Equation (37) is now substituted into (68), thereby selecting a k_a for a desired y^* through (69), and (68) is integrated (we used the Integrate¹⁸ function in Mathematica 10.2 to perform this integral),

$$\bar{f}(y) = \begin{bmatrix} \frac{(k_a - a_1\beta)}{2\omega} - \frac{2k_d(a_1 - a_2c)}{3\pi\omega} \\ \frac{(k_a - a_2\beta)}{2\omega} - \frac{2k_d(a_1(c^2 - s^2) - a_2c^3)}{3\pi\omega} \\ \frac{-2k_d s(2a_2^2 + a_1 a_2 s^2 + 2a_1^2 c)}{3\pi\omega^3 a_1 a_2} \end{bmatrix} \quad (70)$$

where $s := \sin(\omega\delta)$ and $c := \cos(\omega\delta)$. Despite the complexity, we observe the following about the averaged vector field (70):

1. the reflexive $k_d = 0$ case recovers the isolated vertical hopper a_i -dynamics (29) for both hips (first summand in each of the first two rows);

2. when $\delta = 0$ and $a_1 = a_2$, we also recover isolated vertical hopper dynamics in the first two rows, suggesting that behavior close to the equilibrium resembles that of independent vertical hoppers;
3. in the Appendix, we provide an interpretation of the last row as a proportional controller on the phase difference, δ .

The averaged vector field (70) evaluates to 0 at y^* , satisfying Theorem 2(ii). Moreover, we can calculate the Jacobian and evaluate at y^* to obtain

$$D\bar{f}(y^*) = \left[\begin{array}{cc|c} -\zeta_2 - \zeta_3 & \zeta_3 & 0_{2 \times 1} \\ \zeta_3 & -\zeta_2 - \zeta_3 & \\ \hline 0 & & -\frac{8k_d}{3\pi\omega^3} \end{array} \right], \quad (71)$$

where we define the new constants $\zeta_2 := \frac{\beta}{2\omega}$ and $\zeta_3 := \frac{2k_d}{3\pi\omega}$.

4.3.2. Reset. The touchdown condition is the touchdown of hopper 1 after its flight phase, or when $\psi_1 - 1$ (34) crosses zero. As in Section 4.2.2, a_i are not modified by the aerial dynamics. To integrate the aerial dynamics, note first that since the touchdown event is at the zero of $1 - \psi_f^{(1)}$, and $\psi_f^{(1)}(t_{LO}) = 0$, the time of flight is simply $t_f = 1/\omega_f(a_1)$. In this time, hopper 2 must finish its stance phase, complete its flight phase, and proceed through its stance phase (where some of these times may be negative):

$$t_f = \frac{\pi - \psi_v^{(2)}(t_{LO})}{\omega} + \frac{1}{\omega_f(a_2)} + \frac{\psi_v^{(2)}(t_{TD})}{\omega} \quad (72)$$

To express in terms of δ , note that

$$\delta(t_{LO}) = \frac{\pi - \psi_v^{(2)}(t_{LO})}{\omega}, \quad \delta(t_{TD}) = -\frac{\psi_v^{(2)}(t_{TD})}{\omega}$$

Using the above in (72), we obtain

$$\frac{1}{\omega_f(a_1)} = \delta(t_{LO}) - \delta(t_{TD}) + \frac{1}{\omega_f(a_2)}$$

Rearranging, using (35), and putting together with the energy coordinates, we obtain

$$\bar{R}(a_1, a_2, \delta) = \left[a_1, \quad a_2, \quad \delta + \frac{2(a_2 - a_1)}{g} \right]^T \quad (73)$$

Just as in Section 4.2.2, y^* in (69) when substituted into the equation above yields $\bar{R}(y^*) = y^*$, satisfying Theorem 2(ii), and we also note that $D\bar{R}$ has a constant $\mathcal{O}(1)$ part, satisfying Theorem 2(i).

Note that unlike the reset map for the anti-phase limit cycle (62), \bar{K} does not appear here, since we only have a single-mode hybrid system in consideration for the in-phase limit cycle.

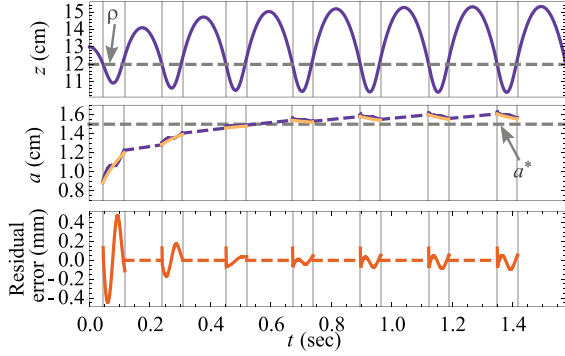


Fig. 4. Top: Displacement of the vertical hopper in physical z coordinates (thin vertical lines separate stance and flight). Middle: Abstract energy coordinate a (29) in purple (dashed: flight) and, in gold, the equivalent continuous dynamical system (43) over several hops. Bottom: Residual error in the a coordinate between trajectories of the averaged and original systems.

4.3.3. *Application of switching averaging.* Using (71) and (73) and evaluating at (69), we obtain the averaged return map

$$\begin{aligned} D\bar{P} &:= D\bar{R} \cdot (I + \varepsilon\pi Df_1) \\ &= \left[\begin{array}{cc|c} 1 - \varepsilon(\zeta_2 + \zeta_3) & \varepsilon\zeta_3 & 0 \\ \varepsilon\zeta_3 & 1 - \varepsilon(\zeta_2 + \zeta_3) & 0 \\ \hline -\frac{2(1-\varepsilon(\zeta_2+2\zeta_3))}{g} & -\frac{2(1-\varepsilon(\zeta_2+2\zeta_3))}{g} & 1 - \frac{\varepsilon 8k_d}{3\pi\omega^2} \end{array} \right] \end{aligned} \quad (74)$$

where ζ_i are as defined in Section 4.3.1. This lower triangular matrix has $1 - \frac{\varepsilon 8k_d}{3\omega}$ as one of its eigenvalues, which is within the unit circle for small $\varepsilon > 0$. The symmetric upper left block has the simple eigenvalues $\{1 - \varepsilon\zeta_2, 1 - \varepsilon\zeta_2 - 2\varepsilon\zeta_3\}$, which are also within the unit circle for small $\varepsilon > 0$. Moreover, $D\bar{P}$ is hyperbolic, and using Theorem 3, we conclude that the pair of independent hoppers has a stable in-phase limit cycle ε close to (69).

5. Numerical results

In this section we present simulation results of the model systems discussed in this paper. In Section 5.1, we display overlapping traces of “unaveraged” and “averaged” dynamics on an isolated vertical hopper, showing the correspondence that is formally established by Theorem 1. In Section 5.2, we demonstrate the efficacy of the new coordination controllers introduced in Section 3.3 on a pair of informationally coupled, mechanically decoupled vertical hoppers.

We would like to remind the reader that the companion paper (De and Koditschek, 2018) contains a much larger swath of not just numerical but also empirical results benefitting from the theoretical contributions of this paper.

5.1. 1-DOF vertical hopper

Using parameters $\omega = 50$ rad/s, $k = 0.4$ N-s/m², $\beta = 10$ N/(m/s) and $\varepsilon = 2$, numerical simulations of the vertical hopper with Mathematica 10, using NDSolve¹⁹ and WhenEvent²⁰ show that

1. the fixed point of the averaged system is approximately 0.15 mm away from the original system’s fixed point (Figure 4 middle, difference between purple a and dashed gray a^*); and
2. the residual error between trajectories of the averaged and original systems are an order of magnitude smaller than $a^* = k/\beta = 0.04$ m (Figure 4, bottom).

Remark 7 (Approximating continuous control with discrete steps). Note that the averaged vector field (43) has the form of a proportional controller on total energy. Thus, Theorem 1 enables us to conclude that the cumulative control effect on body height from multiple isolated steps through a second-order ordinary differential equation (ODE) is approximately equivalent to that of a first-order ODE acting on body height (as shown in Figure 4(middle)); the gold traces in the middle plot correspond to the averaged system and “snipping away” the resets recovers a smooth energy dynamics corresponding to (43).

5.2. Pair of vertical hoppers

In Figure 5 we illustrate numerically the analytical results just derived in Section 4.2–4.3. The physical model we use is the pair of vertical hoppers of Figure 3, and we demonstrate that our new phase controller (38) can stabilize both anti-phase and in-phase limit cycles by changing the sign of the scalar parameter k_d .

We provide empirical demonstration of the phase controller on a physical platform as well as empirical application of the attitude controller (39) in the companion paper (De and Koditschek, 2018) in the “feedback synchronization” empirical results section.

We also show in the Appendix how the phase controller (38) behaves in closed-loop like an abstract phase control such as previously analyzed in Klavins et al. (2000). The empirical benefit of (38) is that it is a smooth function of data $\phi, \dot{\phi}$ measured from sensors on the robot, whereas the abstract phase difference (36) is not only an involved calculation, but also a discontinuous function of the physical state.

6. Conclusion

This paper presents, to the best of our knowledge, the first instance of a generalization to hybrid systems of a classical averaging result. Thus, Theorem 1 joins a growing body of cases wherein suitably constructed hybrid systems (Burden et al., 2016, 2015; Eldering and Jacobs, 2016; Ames and Sastry, 2006; Westervelt et al., 2003; Posa et al., 2016) admit an appropriately restated version of classical

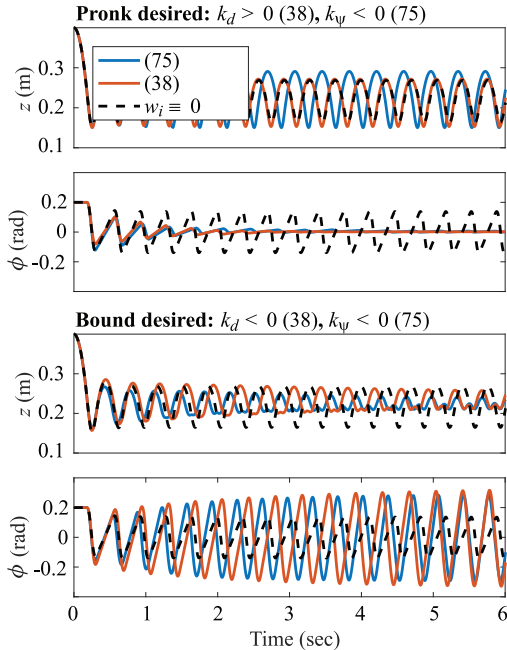


Fig. 5. Comparison of coordination through pure “abstract” phase (75) versus its perceptually direct surrogate (38). Simulation runs of a pair of independent vertical hoppers with $z = (z_1 + z_2)/2$ (Figure 3) where, comparing no phase control (dashed black), the abstract phase control (75) (blue), and our new phase controller (38) (red) that introduces complexity in our analysis here, but leads to more simple and robust physical implementation in (De and Koditschek, 2018). Note that the sign of k_ψ is the same for both limit cycles due to our local definition of δ , as discussed after (55). We also include (dashed black) “baseline” traces with the phase control (38) silenced to demonstrate the behavioral efficacy of either phase control strategy: note the resulting attenuated (top) and accentuated (bottom) pitching with respect to the baseline.

dynamical systems results, with useful applications to new engineering settings.

6.1. Relaxing and extending the required conditions

We provide some examples that demonstrate limitations of the present theory, and in doing so, motivate future theoretical work.

6.1.1. Extension to multiple domains. Intuitively, the ε -parameterization of the continuous dynamics in (1) ensures that all non-phase coordinates vary slowly with respect to the phase. Robotic systems in steady-state operation, with asymptotically stable limit cycles, are one (important) class of systems our results apply to, but by no means the only.

An additional limitation in our modeling is the single continuous mode and reset of (19). Generalizing the results herein to hybrid systems with multiple modes or overlapping guards presents a number of challenges. With multiple

domains, there is no privileged set of coordinates shared across disjoint portions of state space, so it is not obvious how to parameterize the flow to the form of (1). With overlapping guards, the return map is generally discontinuous (Remy et al., 2010, Table 3) or at least nonsmooth (Burden et al., 2016, Section 4.2), so it is not obvious how to generalize conditions on the guard and reset in Theorem 3.

6.1.2. Effects of ε -perturbation. As discussed in Remark 3, large- ε limits of classical averaging conclusions can be found in the literature (e.g. Tsatsos, 2006, 17). Numerically, as well as from our empirical experience in De and Koditschek (2015a), the vertical hopper example in Section 4.1 retains the asymptotic behavior of (43) for large ε (Section 5.1).

6.1.3. Rank condition in Theorems 2(ii) and 3(iii). We emphasize that this condition is necessary for averaging along the lines of hyperbolicity in the classical theory (Guckenheimer and Holmes, 1990, Theorem 4.1.1). Indeed, consider the switching system with flow-time T , dynamics

$$\dot{x} = -\varepsilon x, \quad R(x, \sigma) = x + \varepsilon T x$$

and observe that $\bar{f} = -x$ and $D\bar{f} = -1$. Note that the linearization of the return map,

$$D\bar{R} \cdot D\bar{Q}(x) = (1 + \varepsilon T)(1 - \varepsilon T) + \mathcal{O}(\varepsilon^2) = 1 + \mathcal{O}(\varepsilon^2)$$

is not hyperbolic to $\mathcal{O}(\varepsilon)$, so we cannot assess stability using Theorem 2.

6.2. Applications and extensions in higher dimensions

Application to a simple 1-DOF model relevant to legged locomotion (Section 4.1) indicates that stability analyses of limit cycles in higher-dimensional systems (De and Koditschek, 2015b; Kenneally et al., 2016) could be greatly simplified, in analogy to the simple construction afforded by De and Koditschek (2015a) relative to the initial controllers of De and Koditschek (2015b). This is an avenue of ongoing research being undertaken by the authors, and would add to the large body of emerging engineering-motivated research to develop approximations of the behavior of nonlinear dynamical systems near reference trajectories (Ames et al., 2014; Manchester, 2011; Rijnen et al., 2016; Wu and Sreenath, 2015) (limit cycles in the case of this paper).

In current and future work, we wish to apply this method to systems of much higher dimensionality than considered here or in the companion paper (De and Koditschek, 2018). We believe that the following insights will be key in generalizing this method.

- **Time-reversal symmetry.** As we observe in the last paragraph of Section 4.1.1, the averaging method bears a particular synergy with phase symmetry. The prevalence of symmetry in locomotion (Altendorfer et al.,

2004; Raibert, 1986; Razavi et al., 2016) motivates and encourages further application of the methods introduced here. Work currently in progress reveals that time-reversal symmetry can help find averageable coordinates for a class of hybrid dynamical systems appearing in legged locomotion (such as the examples here), easing the work of representing the continuous dynamics in the form of Theorem 2.

- **Conservation laws.** High-dimensional systems often exhibit symmetries leading to conservation laws, as seen for instance in SLIP or lateral leg spring (LLS) (Holmes et al., 2006). Conservation laws can be leveraged for dimension reduction before application of our hybrid averaging ideas in this paper, especially since conserved quantities contribute to non-hyperbolicity in the return map, thereby precluding the application of Theorem 2.
- **Dimension reduction using feedback anchoring.** The traditional view of anchoring (Full and Koditschek, 1999), or (hybrid) zero dynamics (Westervelt et al., 2003), is that of dimension reduction in the form of an attracting invariant submanifold of the original system. We foresee that our averaging ideas could be applied to the restricted dynamics (“template dynamics” or “zero dynamics”), i.e. after an initial reduction (anchoring) due to passive mechanics or stabilizing feedback control.

Acknowledgement

The authors would like to acknowledge Dr John Guckenheimer for a personal communication that greatly aided our interpretation of Theorem 1, and suggested our new Lemma 1.

Funding

The author(s) disclosed receipt of the following financial support for the research, authorship, and/or publication of this article: This work was supported in part by the NSF (grant number 1028237), in part by the US Army Research Laboratory and the US Army Research Office (contract/grant number W911NF-16-1-0158 awarded to the second author), and in part by the ONR (grant number N00014-16-1-2817), a Vannevar Bush Fellowship held by the last author, sponsored by the Basic Research Office of the Assistant Secretary of Defense for Research and Engineering.

Notes

1. Note that we evaluate at $\varepsilon = 0$ since these terms interact with a Taylor expansion at $\varepsilon = 0$ of \dot{y} , as shown in (6).
2. There was a typo in Guckenheimer and Holmes (1990); it should have said $D\bar{f}(p_0)$ instead of $Df(p)$.
3. This statement means that if p_0 is a hyperbolic fixed point of \bar{f} , by definition, the eigenvalues of $D\bar{f}(p_0)$ have a non-zero real part. Consequently, the eigenvalues of $\exp(\varepsilon T D\bar{f}(p_0))$ do not lie on the unit circle.
4. There was a typo in Guckenheimer and Holmes (1990); not ε^2 -close.
5. Intuitively, the result of (i) holds over a time interval of $\mathcal{O}(1/\varepsilon)$. This statement says that since T does not depend on ε , for small enough ε , the $\mathcal{O}(1/\varepsilon)$ time interval over which (i) applies can be greater than T .
6. The $1/\varepsilon$ in ζ is there to maintain invertibility even as $\varepsilon \rightarrow 0$, since $\lim_{\varepsilon \rightarrow 0} DP_\varepsilon \rightarrow I$.
7. This can be done without loss of generality by scaling γ as long as $D_\sigma \gamma \neq 0$, which we assert as a condition on the transversality of the flow and the guard.
8. We use the term “equivalent” to denote a correspondence stronger than conjugacy; whereas the flows are indeed conjugate, the return maps are identical.
9. This initial condition corresponds to the nominal impact time, not the initialization of the continuous dynamics at $\sigma = 0$. In addition, the reader should note that we keep “ x ” arbitrary for now, i.e. the following calculations hold for any x .
10. We envision that exploiting within-stance time-reversal symmetry as in Altendorfer et al. (2004) could augment the method in this paper, for further analytical benefit (as we pursue with work already in progress seeking to analyze the composition of this paper’s in-place behaviors with the fore-aft motions treated as disturbances in the “empirical compositions” section in De and Koditschek (2018)).
11. The discontinuity of (36) across modes does not introduce any analytical issues as discussed in Remark 6.
12. From (34), $-k_a \omega \cos \psi_i = (\varepsilon k_a / a_i) \dot{z}_i$ (forcing in the direction of velocity, but normalized by a_i).
13. Though the arguments of (38) seemingly involve only physical coordinates, we justify the use of the term *phase controller* by exposing the strong relation between the energetically relevant “proportional/dissipative” form of (38)–(39), and abstract phase control in the Appendix.
14. In addition, in the companion paper (De and Koditschek, 2018), we numerically and empirically test these controllers on systems with preflexive stabilization as well (though we omit these analyses of combined preflexive–feedback stabilization for sake of space and clarity).
15. We remind the readers of the distinction between an integrable flow, and the averaging integral (2). In the latter case, we integrate the vector field over a single “phase” parameter while holding the other states constant.
16. A function f such that $-f(x) = f(-x)$ is *odd* in x , and one such that $f(-x) = f(x)$ is *even* in x .
17. Practitioners may wish to note that ε -closeness in state corresponds to ε -closeness in energy in mechanical systems like this hopper.
18. See <https://reference.wolfram.com/language/ref/Integrate.html>
19. See <http://reference.wolfram.com/language/ref/NDSolve.html>
20. See <https://reference.wolfram.com/language/ref/WhenEvent.html>

References

- Abraham R, Marsden J and Ratiu T (1988) *Manifolds, Tensor Analysis, and Applications (Applied Mathematical Sciences, vol. 75)*. New York: Springer.
- Altendorfer R, Koditschek DE and Holmes P (2004) Stability analysis of legged locomotion models by symmetry-factored return maps. *The International Journal of Robotics Research* 23(10–11): 979–999.
- Ames AD, Galloway K, Sreenath K and Grizzle JW (2014) Rapidly exponentially stabilizing control lyapunov functions

- and hybrid zero dynamics. *IEEE Transactions on Automatic Control* 59(4): 876–891.
- Ames AD and Sastry S (2006) Hybrid Routhian reduction of Lagrangian hybrid systems. In: *American Control Conference (ACC)*. DOI: 10.1109/ACC.2006.1656621.
- Blickhan R and Full R (1993) Similarity in multilegged locomotion: bouncing like a monopode. *Journal of Comparative Physiology A* 173(5): 509–517.
- Burden S, Revzen S and Sastry S (2015) Model reduction near periodic orbits of hybrid dynamical systems. *IEEE Transactions on Automatic Control* 60(10): 2626–2639.
- Burden S, Sastry S, Koditschek D and Revzen S (2016) Event-selected vector field discontinuities yield piecewise-differentiable flows. *SIAM Journal on Applied Dynamical Systems* 15(2): 1227–1267.
- De A (2017) *Modular Hopping and Running via Parallel Composition*. PhD Thesis, University of Pennsylvania. https://repository.upenn.edu/ese_papers/794/.
- De A and Koditschek DE (2015a) Averaged anchoring of decoupled templates in a tail-energized monopod. In: *International Symposium on Robotics Research*. Available at: <http://kodlab.seas.upenn.edu/Avik/AveragingTSLIP>.
- De A and Koditschek DE (2015b) Parallel composition of templates for tail-energized planar hopping. In: *2015 IEEE International Conference on Robotics and Automation (ICRA)*, pp. 4562–4569.
- De A and Koditschek DE (2018) Vertical hopper compositions for preflexive and feedback-stabilized quadrupedal bounding, pronking, pacing and trotting. In press.
- Eldering J and Jacobs HO (2016) The role of symmetry and dissipation in biolocomotion. *SIAM Journal on Applied Dynamical Systems* 15(1): 24–59.
- Full RJ and Koditschek DE (1999) Templates and anchors: neuromechanical hypotheses of legged locomotion on land. *Journal of Experimental Biology* 202(23): 3325–3332.
- Geyer H, Seyfarth A and Blickhan R (2006) Compliant leg behaviour explains basic dynamics of walking and running. *Proceedings of the Royal Society B: Biological Sciences* 273(1603): 2861–2867.
- Guckenheimer J and Holmes P (1990) *Nonlinear Oscillations, Dynamical Systems, and Bifurcations of Vector Fields (Applied Mathematical Sciences)*. New York: Springer.
- Hirsch M, Devaney R and Smale S (1974) *Differential Equations, Dynamical Systems, and Linear Algebra (Pure and Applied Mathematics)*. Amsterdam: Elsevier Science.
- Holmes P, Full RJ, Koditschek D and Guckenheimer J (2006) The dynamics of legged locomotion: Models, analyses, and challenges. *SIAM Review* 48(2): 207–304.
- Johnson AM, Burden SA and Koditschek DE (2016) A hybrid systems model for simple manipulation and self-manipulation systems. *The International Journal of Robotics Research* 35(11): 1354–1392.
- Kenneally G, De A and Koditschek DE (2016) Design principles for a family of direct-drive legged robots. *IEEE Robotics and Automation Letters* 1(2): 900–907.
- Klavins E and Koditschek DE (2002) Phase regulation of decentralized cyclic robotic systems. *The International Journal of Robotics Research* 21(3): 257–275.
- Klavins E, Koditschek DE and Ghrist R (2000) Toward the Regulation and Composition of Cyclic Behaviors. In: Donald B, Lynch K and Rus D (eds.) *Algorithmic and Computational Robotics: New Directions 2000 WAFR*. Wellesley: A.K. Peters, pp. 205–220.
- Koditschek DE and Buehler M (1991) Analysis of a simplified hopping robot. *The International Journal of Robotics Research* 10(6): 587–605.
- Manchester IR (2011) Transverse dynamics and regions of stability for nonlinear hybrid limit cycles. *IFAC Proceedings Volumes* 44(1): 6285–6290.
- Posa M, Tobenkin M and Tedrake R (2016) Stability analysis and control of rigid-body systems with impacts and friction. *IEEE Transactions on Automatic Control* 61(6): 1423–1437.
- Poulakakis I (2006) On the stability of the passive dynamics of quadrupedal running with a bounding gait. *The International Journal of Robotics Research* 25(7): 669–687.
- Proctor J, Kukillaya RP and Holmes P (2010) A phase-reduced neuro-mechanical model for insect locomotion: feed-forward stability and proprioceptive feedback. *Philosophical Transactions of the Royal Society A: Mathematical, Physical and Engineering Sciences* 368(1930): 5087–5104.
- Raibert M (1986) *Legged Robots that Balance*. Artificial Intelligence. Cambridge, MA: MIT Press.
- Raibert MH, Brown Jr HB, Chepponis M, et al. (1989) *Dynamically Stable Legged Locomotion* (September 1985–September 1989). Available at: <https://dspace.mit.edu/handle/1721.1/6820>.
- Razavi H, Bloch AM, Chevallereau C and Grizzle JW (2016) Symmetry in legged locomotion: a new method for designing stable periodic gaits. *Autonomous Robots*.
- Remy CD, Buffinton K and Siegwart R (2010) Stability analysis of passive dynamic walking of quadrupeds. *The International Journal of Robotics Research* 29(9): 1173–1185.
- Rijnen M, van Rijn A, Dallali H, Saccon A and Nijmeijer H (2016) Hybrid trajectory tracking for a hopping robotic leg. *IFAC-PapersOnLine* 49(14): 107–112.
- Saranli U, Schwind WJ and Koditschek DE (1998) Toward the control of a multi-jointed, monopod runner. In: *1998 IEEE International Conference on Robotics and Automation*, volume 3, pp. 2676–2682.
- Schmitt J and Holmes P (2000) Mechanical models for insect locomotion: dynamics and stability in the horizontal plane I. Theory. *Biological Cybernetics* 83(6): 501–515.
- Shahbazi M and Lopes GAD (2016) Coordination of monopodal SLIP models towards quadrupedal running. In: *2016 IEEE/RSJ International Conference on Intelligent Robots and Systems (IROS)*, Daejeon, Korea.
- Tsatsos M (2006) *Theoretical and numerical study of the Van der Pol equation*. Doctoral dissertation, Aristotle University of Thessaloniki.
- Van Der Schaft AJ and Schumacher JM (2000) *An introduction to hybrid dynamical systems*, volume 251. London: Springer.
- Westervelt ER, Grizzle JW and Koditschek DE (2003) Hybrid zero dynamics of planar biped walkers. *IEEE Transactions on Automatic Control* 48(1): 42–56.
- Wu G and Sreenath K (2015) Variation-based linearization of nonlinear systems evolving on $SO(3)$ and S^2 . *IEEE Access* 3: 1592–1604.

Appendix: A physical surrogate for abstract phase difference (Section 3.3)

This appendix contains various calculations that are used for our stability proofs, broken down by the section in which they appear.

In each of Sections 4.2–4.3, a more straightforward proof involving algebraically simpler terms could have been obtained by introducing instead of (38) a coordination term based upon the abstract phase difference

$$w_i(x) = (-1)^{i-1} k_\psi \sin \psi_i \sin(\omega\delta) \quad (75)$$

as in Klavins et al. (2000, equation (7)). This is because in both of the preceding averaging analyses, δ is shown to be a “slow” coordinate ($\dot{\delta} = \mathcal{O}(\varepsilon)$), and can be held constant while performing the averaging integral in (56) and (70).

However, the analytically simpler alternative (75) requires computation of the abstract phase difference δ for implementation, which is quite involved (36), especially due to the discontinuities in its definition across modes. In comparison, our globally well-defined phase controller (38) is a simple function of the physical variables that can be easily measured with sensors. We observe in Appendix A.1 that, notwithstanding its simplicity, the coordination controller (38) actually functions as a physical surrogate for the abstract phase difference, behaving, in both the in-phase and anti-phase cases, like a proportional phase controller *in the averaged sense*. We then discuss the numerical and empirical utility of this simply implemented surrogate in Appendix A.2.

Although a matter of considerable conceptual interest, we are not aware of an analogously equivalent “abstract” version of the attitude controller (39) that is a function of the ψ_i coordinates only.

A.1. Closed-loop phase-difference dynamics

Though our phase controller (38) looks quite different from the abstract version (75):

1. an inspection of the last row of (56) reveals that $\dot{\delta} \overset{\text{avg}}{\propto} -\delta$; and
2. inspection of the $\sin(\omega\delta)$ factor in (or application of the Series function in Mathematica to) the last row of (70) reveals that $\dot{\delta} \overset{\text{avg}}{\propto} -\delta(a_1^2 + a_2^2) + \mathcal{O}(\delta^2)$;

where we use the $\overset{\text{avg}}{\propto}$ symbol and omit constant positive parameters, but include all functions of state explicitly. In both cases, the closed-loop δ dynamics take the form of a proportional control on δ for small δ , which is identical to (75).

A.2. Numerical comparison

Figure 5 shows a numerical comparison between the abstract phase control (75) and the approximation (38) for both positive and negative signs of the gain k_d , respectively stabilizing a bounding and a pronking limit cycle in a pair of independent hoppers.

In the companion paper (De and Koditschek, 2018), we show in simulation our approximated phase control applied to coupled vertical hoppers and, more importantly, on the physical platform. Our results show that (38) is able to overcome reflexive stability and stabilize the physical platform leg phases to a desired limit cycle for trotting and pacing, as well as to obtain bounding or pronking.